LETTER

doi:10.1038/nature24998

A non-canonical Notch complex regulates adherens junctions and vascular barrier function

William J. Polacheck[1,2]*, Matthew L. Kutys[1,2]*, Jinling Yang[1,2], Jeroen Eyckmans[1,2], Yinyu Wu[3], Hema Vasavada[3], Karen K. Hirschi[3] & Christopher S. Chen[1,2]

The vascular barrier that separates blood from tissues is actively regulated by the endothelium and is essential for transport, inflammation, and haemostasis[1]. Haemodynamic shear stress plays a critical role in maintaining endothelial barrier function[2], but how this occurs remains unknown. Here we use an engineered organotypic model of perfused microvessels to show that activation of the transmembrane receptor NOTCH1 directly regulates vascular barrier function through a non-canonical, transcription-independent signalling mechanism that drives assembly of adherens junctions, and confirm these findings in mouse models. Shear stress triggers DLL4-dependent proteolytic activation of NOTCH1 to expose the transmembrane domain of NOTCH1. This domain mediates establishment of the endothelial barrier; expression of the transmembrane domain of NOTCH1 is sufficient to rescue defects in barrier function induced by knockout of *NOTCH1*. The transmembrane domain restores barrier function by catalysing the formation of a receptor complex in the plasma membrane consisting of vascular endothelial cadherin, the transmembrane protein tyrosine phosphatase LAR, and the RAC1 guanidine-exchange factor TRIO. This complex activates RAC1 to drive assembly of adherens junctions and establish barrier function. Canonical transcriptional signalling via Notch is highly conserved in metazoans and is required for many processes in vascular development, including arterial–venous differentiation[3], angiogenesis[4] and remodelling[5]. We establish the existence of a non-canonical cortical NOTCH1 signalling pathway that regulates vascular barrier function, and thus provide a mechanism by which a single receptor might link transcriptional programs with adhesive and cytoskeletal remodelling.

The selective barrier formed by the monolayer of vascular endothelial cells that lines blood vessels prevents tissue oedema and maintains plasma volume, while enabling exchange of immune cells and nutrients with surrounding tissue across the endothelium, in part through the dynamic regulation of endothelial cell–cell junctions. Dysfunction in barrier maintenance is a hallmark of, and is often the underlying cause of, many cardiovascular pathologies. While a host of soluble factors including growth factors, circulating lipids, and reactive oxygen species transmit chemical signals to endothelial cells, haemodynamic forces regulate vascular permeability locally and acutely by remodelling endothelial cell–cell junctions and the cytoskeleton[6]. The shear stress caused by steady laminar flow improves the integrity of the barrier by stabilizing cell–cell junctions, while perfusion defects increase vascular permeability and contribute to the pathogenesis of cardiovascular diseases such as atherosclerosis[7], stroke[8] and myocardial infarction[9]. While *in vitro* studies have identified putative shear-stress-responsive signalling pathways that mediate endothelial junction and cytoskeletal remodelling[7], the mechanisms that link haemodynamic shear stress to the regulation of endothelial cell–cell junctions and vascular permeability remain unknown.

In vivo mechanistic studies of the influence of shear stress on the vascular barrier are challenging, because control over pressures and flows is limited, and the effects of shear stress cannot be decoupled from changes in nutrient exchange. *In vitro* approaches have enabled better control of these forces, but the use of stiff, planar substrates for cell culture artificially influences cell–extracellular matrix (ECM) and cell–cell adhesion signalling. We therefore developed human engineered microvessels (hEMVs), a biomimetic model of the microvasculature consisting of a lumen surrounded by ECM, lined with human dermal microvascular endothelial cells (Fig. 1a), and connected to a microfluidic device to enable precise control of perfusion and haemodynamic stresses. This simplified model lacks other cell types such as pericytes or tissue-specific parenchyma, and therefore focuses on autonomous functions of the endothelium. Consistent with *in vivo* observations[2], the endothelial lining of hEMVs in the absence of flow was leaky, allowing fluorescently labelled 70-kDa dextran to diffuse from the lumen into the interstitial matrix, whereas steady perfusion at flow rates that impart physiological shear stress to the endothelial cells (>3 dyn cm^{-2}) promoted the establishment of a functional vascular barrier that was resistant to leakage and sensitive to known permeability factors (Fig. 1b, c, Extended Data Fig. 1a–e).

Shear stress regulates numerous mechanosensitive pathways whose signatures can be inferred from the upregulation of various genetic networks both *in vivo* and *in vitro*[10]. We observed increased expression of many such genes in our hEMV system, but noted numerous genes associated with Notch signalling, including those encoding the NOTCH1 ligand DLL4 and the downstream targets of NOTCH1 activation HES1 and HEY1 (Fig. 1d, Extended Data Fig. 2). Activation of Notch signalling by shear stresses has recently been shown in zebrafish[11], so to investigate whether Notch signalling was also involved in shear-induced barrier function in the hEMV system, we treated hEMVs with DAPT (*N*-[*N*-(3,5-difluorophenacetyl)-L-alanyl]-*S*-phenylglycine *t*-butylester), an inhibitor of γ-secretase[4], which cleaves NOTCH1 to release the transcriptionally active intracellular domain (ICD) of NOTCH1 (Extended Data Fig. 3a)[12]. Cleavage of ICD from NOTCH1 increased with flow (Fig. 1e), and treatment with DAPT in the presence of shear increased permeability (Fig. 1f). Conversely, directly activating NOTCH1 by coating the ablumenal surface of the microvessel with recombinant DLL4 (rDLL4, Extended Data Fig. 3a, b) before cell seeding reduced permeability even in static (no flow) conditions (Fig. 1f). Examination of the endothelium confirmed that shear stress reduced permeability by inducing the assembly of adherens junctions containing vascular endothelial (VE)-cadherin (encoded by *CDH5*) and the redistribution of F-actin to the cortical membrane (Fig. 1g, h). The integrity of this organization was disrupted by DAPT (Fig. 1g, h), and NOTCH1 activation by rDLL4 phenocopied the shear-induced phenotype (Extended Data Fig. 3c).

Canonical Notch signalling occurs through ICD-dependent transcription of downstream Notch target genes[13]. To identify the role of Notch transcriptional signalling in regulating barrier function, we seeded hEMVs with cells expressing a dominant-negative form of the Notch transcriptional co-factor mastermind-like protein 1

[1]The Wyss Institute for Biologically Inspired Engineering, Harvard University, Boston, Massachusetts, USA. [2]The Biological Design Center and Department of Biomedical Engineering, Boston University, Boston, Massachusetts, USA. [3]Yale Cardiovascular Research Center, Departments of Internal Medicine, Genetics, and Biomedical Engineering, New Haven, Connecticut, USA.
*These authors contributed equally to this work.

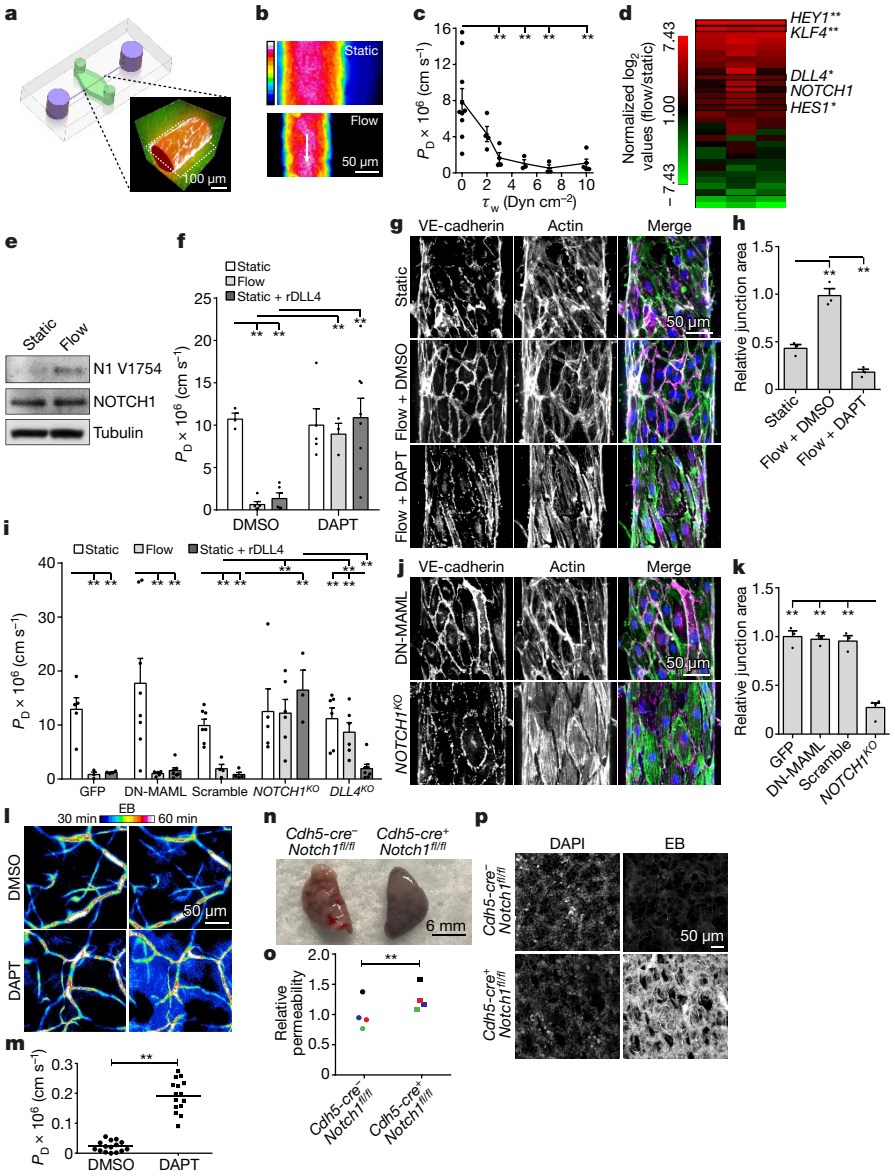

Figure 1 | NOTCH1 regulates shear stress-induced vascular barrier function. a, Organotypic microfluidic hEMV devices consisting of human endothelial cells (red) in physiological ECM (green) enables vessel perfusion at a defined luminal shear stress (purple, inlet and outlet). Inset, 3D reconstruction of hEMVs. Red, 70-kDa dextran; white, VE-cadherin; green, collagen I. **b**, Real-time assessment of vascular barrier function in hEMVs cultured statically or under flow (heat map of fluorescence intensity of 70-kDa dextran, imaging plane indicated by dashed line in **a**. **c**, Quantification of the diffusive permeability (P_D) of 70-kDa dextran across the endothelial cell barrier as a function of endothelial-wall shear stress (τ_w). **d**, Relative gene expression of endothelial cells cultured in static or flow conditions quantified by qPCR; NOTCH1 target genes that are regulated by flow are indicated. Each column represents an independent experiment; for full gene panel see Extended Data Fig. 2. **e**, ICD cleavage in lysates of endothelial cells cultured in static and flow conditions as measured by western blot with an antibody specific to cleaved ICD (N1 V1754). **f**, Diffusive permeability measured in hEMV cultures in static or flow conditions in the presence of DAPT or rDLL4-coated collagen (rDLL4). **g**, Fluorescent micrographs of hEMVs immunostained for VE-cadherin (magenta) and labelled with DAPI (blue) and the actin stain phalloidin (green). **h**, Quantification of junctional area measured from micrographs of cells immunostained for VE-cadherin. **i**, Diffusive permeability of hEMVs cultured in static or flow conditions, or on rDLL4-coated collagen with endothelial cells expressing dominant-negative MAML (DN-MAML), GFP control, or with *NOTCH1*^{KO}, *DLL4*^{KO} or scramble control (Scr) endothelial cells. **j**, Fluorescence micrographs showing actin and VE-cadherin staining in hEMV cultures under flow with endothelial cells expressing DN-MAML or with *NOTCH1*^{KO} endothelial cells. **k**, Quantification of junctional area measured in cells immunostained for VE-cadherin as shown in **j**. Corresponding micrographs for GFP and scramble controls are shown in Extended Data Fig. 3. In **a**–**k**, $n \geq 3$ independent hEMVs, mean ± s.e.m. **l**, Heat maps of Evans blue fluorescence in the mouse dermal vasculature 30 min and 60 min after intravenous co-injection with DAPT or DMSO vehicle control. **m**, Quantification of diffusive permeability of Evans blue diffusion into the dermal interstitial space ($n = 15$ vessels across 3 mice per condition). **n**, Lungs harvested from mice killed 30 min after intravenous injection of Evans blue. **o**, Vascular permeability was quantified by eluting and measuring the concentration of dye in the lungs relative to the concentration in the blood ($n = 4$ age and sex-matched littermates; colour-coded, two-way ANOVA). **p**, Whole-mount lung vasculature immunostains showing leaked Evans blue and stained with DAPI. $^*P < 0.05$, $^{**}P < 0.01$; exact P and n values are shown in Source Data; all images are representative of at least three independent experiments.

(DN-MAML)[14]. Unexpectedly, DN-MAML expression did not affect permeability (Fig. 1i) or adherens junction formation (Fig. 1j, k, Extended Data Fig. 3d), despite inhibiting Notch transcriptional signalling (Extended Data Fig. 3e). To investigate potential non-canonical mechanisms by which Notch activity could regulate barrier function, we generated hEMVs with cells harbouring CRISPR–Cas9-mediated knockout of *NOTCH1* and *DLL4* (*NOTCH1*^{KO}, Extended Data Fig. 3f; *DLL4*^{KO}, Extended Data Fig. 4a). *NOTCH1*^{KO} cells phenocopied DAPT

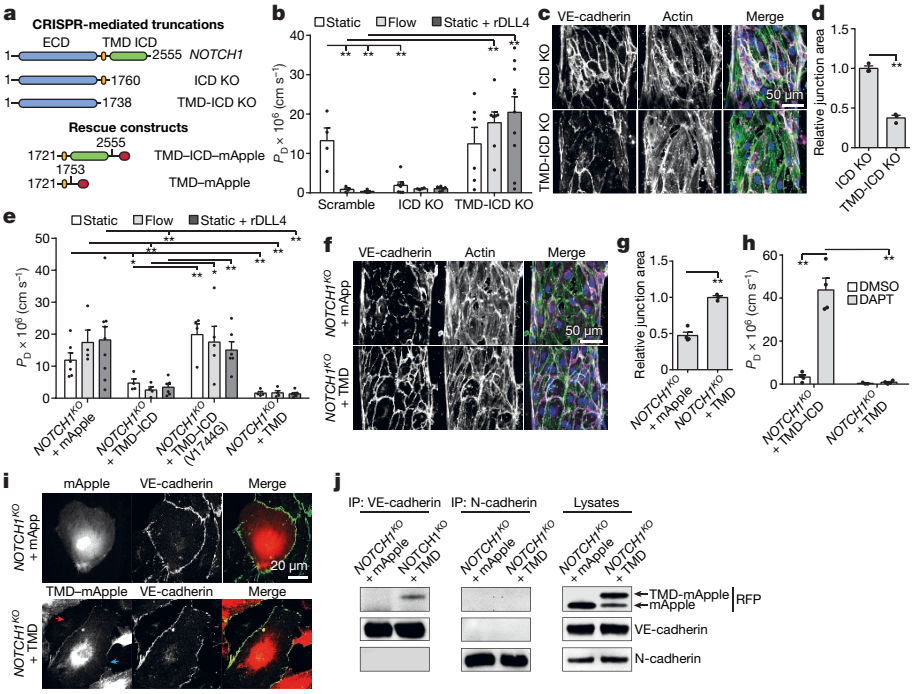

Figure 2 | The NOTCH1 transmembrane domain mediates barrier function through interaction with VE-cadherin. a, A library of endogenous *NOTCH1* truncation mutants and overexpression rescue constructs were generated to examine the key functional domains of NOTCH1 that regulate barrier function. **b**, Diffusive permeability for endothelial cells with CRISPR–Cas9-mediated endogenous truncation of NOTCH1 ICD (ICD KO) or truncation of the TMD and ICD (TMD-ICD KO) cultured in static or flow conditions, or in the presence of rDLL4-coated collagen. **c**, Fluorescent micrographs of VE-cadherin and actin for ICD KO and TMD-ICD KO endothelial cells under flow conditions. **d**, Quantification of junctional area measured from VE-cadherin-immunostained micrographs. **e**, Diffusive permeability of *NOTCH1*^{KO} endothelial cells expressing TMD–ICD–mApple, TMD–ICD(V1754G)–mApple, TMD–mApple, or mApple infection control cultured in static or flow conditions, or in the presence of rDLL4-coated collagen. **f**, Fluorescent micrographs of VE-cadherin (magenta), actin (green), and DAPI (blue) in static *NOTCH1*^{KO} cells expressing TMD–mApple or mApple infection control. **g**, Quantification of junctional area measured from VE-cadherin-immunostained micrographs as shown in **f**. **h**, Diffusive permeability for static *NOTCH1*^{KO} cells expressing TMD–ICD–mApple or ICD–mApple exposed to DAPT or DMSO control. **i**, Immunofluorescent images of *NOTCH1*^{KO} cells expressing either mApple or TMD–mApple, co-stained for VE-cadherin. Co-localization of the NOTCH1 TMD and VE-cadherin (red arrow) is lost at free edges (blue arrow). **j**, Immunoprecipitation of VE-cadherin and N-cadherin from *NOTCH1*^{KO} cells expressing either mApple or TMD–mApple. Immunoblotting with an RFP antibody identified TMD–mApple in the immunoprecipitates. For all plots, mean ± s.e.m., $n \geq 3$ independent hEMVs, $^*P < 0.05$, $^{**}P < 0.01$. Exact *P* and *n* values are shown in Source Data, all images are representative of at least three independent experiments.

treatment, resulting in increased permeability (Fig. 1i) and impaired adherens junction integrity (Fig. 1j, k, Extended Data Fig. 3h–j) without affecting total VE-cadherin levels (Extended Data Fig. 3j) or cell proliferation (Extended Data Fig. 3k, l). DLL4 was also required for flow-induced barrier formation (Fig. 1i), cleavage of the ICD from NOTCH1 (Extended Data Fig. 4a) and adherens junction formation (Extended Data Fig. 4b, c). Shear stress has been reported to elevate endocytosis in endothelial cells[15], and internalization of DLL4 appears to be necessary for ligand-mediated NOTCH1 activation[16]. We found that flow induced dynamin-dependent internalization of DLL4 (Extended Data Fig. 4d–f), and that chemical inhibition of dynamin reduced DLL4 internalization and abrogated barrier function (Extended Data Fig. 4g). To validate the finding that Notch activation regulates barrier function, we examined the role of Notch signalling in barrier maintenance *in vivo*. DAPT was co-injected intravenously with Evans blue dye into six-to-eight-week-old BALB/c nude mice, and dermal vascular permeability was quantified in real time using intravital microscopy (Fig. 1l, m). Inhibition of Notch signalling with DAPT significantly increased vascular permeability (Fig. 1l, m, Extended Data Fig. 5a). The implication that Notch might regulate barrier function via a transcriptionally independent pathway was consistent with the observation that DAPT increased vascular permeability within 15–60 min *in vivo* (Fig. 1l) and *in vitro* (Extended Data Fig. 6a). This response is likely to be too rapid to be a transcription-dependent response. *In vivo,* knockout of endothelial NOTCH1 resulted in loss of barrier function, increasing vascular permeability in the lung, as assessed by extravasation of Evans blue[17] (Fig. 1n–p, Extended Data Fig. 5b). Together, these results suggest that shear stress has an important role in maintenance of endothelial integrity, and that NOTCH1 might regulate this effect through a non-transcriptional mechanism.

Upon NOTCH1 activation, the extracellular domain (ECD) of NOTCH1 is cleaved, which allows γ-secretase-mediated cleavage of the ICD, leaving the transmembrane domain (TMD) in the plasma membrane[18]. Given the observed increase in ICD cleavage with flow, we generated a library of CRISPR–Cas9-mediated NOTCH1 truncation mutants and recombinant rescue constructs (Fig. 2a, Extended Data Fig. 6e) to determine whether these subdomains of NOTCH1 contributed to the regulation of vascular permeability. Truncation of the ICD (ICD KO) resulted in constitutively low permeability and elaborated adherens junctions (Fig. 2b–d) in static conditions, while truncation of both the ICD and the TMD (ICD-TMD KO) increased permeability under flow (Fig. 2b). These data suggest that the ICD is not critical for NOTCH1-induced barrier function, whereas the TMD is essential. Indeed, expression of the TMD alone or of TMD–ICD in *NOTCH1*^{KO} cells rescued barrier function and adherens junction assembly (Fig. 2e–g). *NOTCH1*^{KO} cells expressing TMD–ICD containing a point mutation that prevents cleavage of the ICD[19] (V1754G, Extended Data Fig. 6b) failed to rescue barrier function (Fig. 2e); and TMD–ICD failed to rescue barrier function in the presence of DAPT, while cells expressing the TMD alone maintained barrier function irrespective of whether they were treated with DAPT (Fig. 2h). Together, these findings are consistent with a model in which the TMD is the essential domain of NOTCH1 for regulating barrier function, and the barrier-forming activity of the TMD requires cleavage of the ICD from

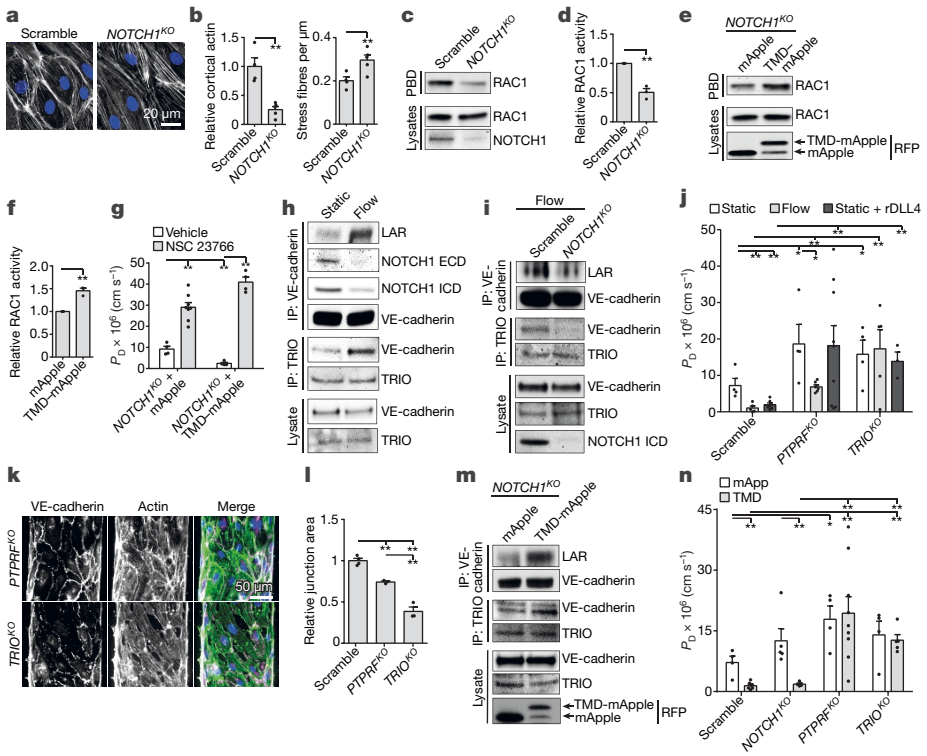

Figure 3 | NOTCH1 assembles a mechanosensory junctional complex involving LAR, TRIO, and RAC. a, Fluorescence micrographs of phalloidin-stained endothelial cells. **b**, Intensity of cortical actin at cell–cell junctions and the number of stress fibres per micrometre, quantified from phalloidin-stained endothelial cells ($n = 3$ hEMVs). **c**, Active RAC1 was isolated from scramble and *NOTCH1*^{KO} cell lysates using the recombinant p21-binding domain of PAK1 (GST–PBD). **d**, Quantification of band intensity from **c** revealed a decrease in RAC1 (~50%) after knockout of *NOTCH1* ($n = 3$ independent lysates). **e**, Active RAC1 was isolated using GST–PBD from lysates of *NOTCH1*^{KO} cells expressing mApple or TMD–mApple. **f**, Quantification of band intensities from **e** shows an increase in RAC1 (~45%) with expression of TMD–mApple ($n = 3$ independent lysates). **g**, Diffusive permeability of *NOTCH1*^{KO} endothelial cells expressing TMD–mApple or mApple control in the presence of 50 μM NSC 23766 (a RAC1 inhibitor) or vehicle control. **h**, Immunoprecipitation of VE-cadherin and TRIO from endothelial cells cultured in static or flow conditions. Co-immunoprecipitation of mechanosensory complex proteins was assessed by immunoblotting for NOTCH1 ECD, NOTCH1 ICD, LAR (85 kDa P subunit) and VE-cadherin. **i**, Immunoprecipitation of VE-cadherin and TRIO from *NOTCH1*^{KO} and scramble control endothelial cells cultured under flow. Co-immunoprecipitation of mechanosensory complex proteins was assessed by immunoblotting for VE-cadherin, LAR, and TRIO. **j**, Diffusive permeability of *PTPRF*^{KO} and *TRIO*^{KO} endothelial cells cultured in static or flow conditions or in the presence of rDLL4-coated collagen. **k**, Micrographs of *PTPRF*^{KO} and *TRIO*^{KO} endothelial cells under flow conditions (magenta, VE-cadherin; green, actin; blue, DAPI). **l**, Quantification of junctional area measured from micrographs of endothelial cells immunostained for VE-cadherin as shown in **k**. **m**, Immunoprecipitation of VE-cadherin and TRIO from *NOTCH1*^{KO} cells expressing TMD–mApple or mApple control. Immunoblotting with antibodies against LAR, VE-cadherin and RFP was used to assess co-immunoprecipitation of mechanosensory complex upon expression of TMD. **n**. Diffusive permeability of *NOTCH1*^{KO}, *PTPRF*^{KO}, *TRIO*^{KO} and scramble control cells cultured under static conditions expressing TMD–mApple or mApple infection control. For **g**, **j**, **n**, $n \geq 3$ hEMVs. All plots, mean ± s.e.m., $^{*}P < 0.05$, $^{**}P < 0.01$. Exact *P* and *n* values are shown in Source Data. All images are representative of at least three independent experiments.

NOTCH1. To our knowledge, the NOTCH1 TMD has not previously been demonstrated to have a biological function.

To investigate the mechanism by which the NOTCH1 TMD contributes to adherens junction assembly, we expressed mApple-tagged TMD in endothelial cells. TMD–mApple localized to cell–cell junctions containing VE-cadherin, and this localization was lost in cells deficient in VE-cadherin (Fig. 2i; Extended Data Fig. 6c, d). VE-cadherin co-immunoprecipitated with NOTCH1 (Extended Data Fig. 6f), and the NOTCH1 TMD specifically co-immunoprecipitated with VE-cadherin, but not with neural (N)-cadherin (encoded by *CDH2*; Fig. 2j), and that this interaction was mediated, in part, by a six-amino-acid stretch in the N-terminal ectodomain of the TMD (Extended Data Fig. 6g, h). These data suggest that the NOTCH1 TMD mediates a specific interaction between NOTCH1 and VE-cadherin.

A possible mechanism by which the NOTCH1 TMD regulates cell–cell junction assembly was suggested by the reduced cortical actin and increased actin stress fibres in *NOTCH1*^{KO} cells (Fig. 3a, b). The Rho-family GTPases are powerful regulators of actin redistribution and barrier function[20], and RAC1 can stabilize adherens junctions by promoting the formation of cortical actin bundles[21]. Indeed, *NOTCH1*^{KO} cells and endothelial cells treated with DAPT exhibited reduced RAC1 activity (Fig. 3c, d, Extended Data Fig. 7a, b), while expression of the NOTCH1 TMD increased RAC1 activity (Fig. 3e, f). RAC1 activity increased with flow (Extended Data Fig. 7c), and this increase in RAC1 activity was abrogated by genetic deletion of NOTCH1 or DLL4 (Extended Data Fig. 7d, e). *NOTCH1*^{KO} cells expressing the NOTCH1 TMD and treated with the RAC1 inhibitor NSC 23766 had increased permeability (Fig. 3g), demonstrating that RAC1 activity was required for barrier function.

To investigate the molecular intermediaries by which NOTCH1 regulates RAC1, we used immunoprecipitation to identify several proteins that interact with VE-cadherin. Only one of these partner proteins, the transmembrane protein tyrosine phosphatase LAR (encoded by *PTPRF*), dissociated from VE-cadherin in *NOTCH1*^{KO} cells (Extended Data Fig. 8a). Notably, LAR has been reported to bind the RAC1 guanine-exchange factor (GEF) TRIO (also known as triple functional domain protein[22]), which has been shown to play a role in Notch-mediated axon guidance in *Drosophila*[23]. Here we demonstrate that LAR mediates a NOTCH1-dependent interaction between TRIO and VE-cadherin (Extended Data Fig. 8b). Under static conditions, full-length NOTCH1 was associated with VE-cadherin (Fig. 3h). Flow-induced activation of NOTCH1 released both the

ECD and the ICD from VE-cadherin and stimulated the interaction of VE-cadherin with LAR and TRIO (Fig. 3h). The formation of the LAR–TRIO–VE-cadherin complex was NOTCH1-dependent *in vitro* (Fig. 3i) and *in vivo* (Extended Data Fig. 8c, d). Using a VE-cadherin biotin ligase proximity-labelling construct[24], we confirmed that the association of ICD with VE-cadherin decreased, and the interaction between TRIO and VE-cadherin increased, with NOTCH1 stimulation (Extended Data Fig. 8e, f). Furthermore, LAR and TRIO are required for the establishment of barrier function, as shown by the reduced RAC1 activity (Extended Data Fig. 7e), high permeability (Fig. 3j), and lack of adherens junctions (Fig. 3k, l) in $PTPRF^{KO}$ and $TRIO^{KO}$ hEMVs. Expression of the TMD rescued the interaction of LAR and TRIO with VE-cadherin (Fig. 3m), and LAR and TRIO were required for NOTCH1 TMD-mediated rescue of barrier defects (Fig. 3n). Thus, cleavage of the ICD from NOTCH1 releases the TMD, enabling it to assemble a complex containing VE-cadherin, LAR, and TRIO, thereby inducing RAC1 activity to assemble junctions and establish barrier function (Extended Data Fig. 9).

Notch signalling is a central regulator of many developmental and homeostatic processes, but its diverse effects have been difficult to explain through just the one canonical pathway involving ICD-dependent transcription of Notch target genes[13]. Here, we have demonstrated that receptor cleavage induced by NOTCH1 activation also brings into play the TMD, which promotes association among transmembrane receptors and signalling molecules and acts as a focal point in a pathway that regulates junction assembly and vascular barrier function. Recent work has shown that interactions between the transmembrane domains of other surface receptors drive signalling in diverse biological contexts[25], suggesting that this is a general mechanism for controlling complex formation at the cell surface.

In the context of Notch, this cortical signalling pathway may explain why human mutations in the Notch receptor family cause vascular defects and barrier dysfunction in human diseases such as CADASIL (cerebral autosomal dominant arteriopathy with subcortical infarcts and leukoencephalopathy), Adams–Oliver syndrome and Alagille syndrome[26–28], and why inhibition of Notch signalling to treat tumours appears to trigger oedema[29]. Identifying ways to isolate the cortical pathway of Notch from the transcriptional pathway may provide new opportunities to control these devastating complications. Furthermore, quantitative differences in expression of Notch and DLL4 in different vascular beds, described as a key mechanism for tip–stalk cell specification in angiogenesis[30], may underlie differences in shear sensitivity and baseline permeability in organ-specific vascular beds. More broadly, the combination of a non-canonical pathway that regulates adhesive and cytoskeletal processes together with a transcriptional regulator of cell-fate programs, channelled through a single receptor, provides a new framework for understanding coordinated developmental programs such as stem-cell differentiation and tissue morphogenesis.

Online Content Methods, along with any additional Extended Data display items and Source Data, are available in the online version of the paper; references unique to these sections appear only in the online paper.

Received 15 May; accepted 6 November 2017.
Published online 13 November 2017.

1. Mehta, D. & Malik, A. B. Signaling mechanisms regulating endothelial permeability. *Physiol. Rev.* **86,** 279–367 (2006).
2. Chiu, J.-J. & Chien, S. Effects of disturbed flow on vascular endothelium: pathophysiological basis and clinical perspectives. *Physiol. Rev.* **91,** 327–387 (2011).
3. Lawson, N. D. *et al.* Notch signaling is required for arterial–venous differentiation during embryonic vascular development. *Development* **19,** 3675–3683 (2001).
4. Hellström, M. *et al.* Dll4 signalling through Notch1 regulates formation of tip cells during angiogenesis. *Nature* **445,** 776–780 (2007).
5. Krebs, L. T. *et al.* Notch signaling is essential for vascular morphogenesis in mice. *Genes Dev.* **14,** 1343–1352 (2000).
6. Li, Y.-S. J., Haga, J. H. & Chien, S. Molecular basis of the effects of shear stress on vascular endothelial cells. *J. Biomech.* **38,** 1949–1971 (2005).
7. Hahn, C. & Schwartz, M. A. Mechanotransduction in vascular physiology and atherogenesis. *Nat. Rev. Mol. Cell Biol.* **10,** 53–62 (2009).
8. Ayata, C. & Ropper, A. H. Ischaemic brain oedema. *J. Clin. Neurosci.* **9,** 113–124 (2002).
9. Dongaonkar, R. M., Stewart, R. H., Geissler, H. J. & Laine, G. A. Myocardial microvascular permeability, interstitial oedema, and compromised cardiac function. *Cardiovasc. Res.* **87,** 331–339 (2010).
10. Garcia-Cardeña, G., Comander, J., Anderson, K. R., Blackman, B. R. & Gimbrone, M. A. Jr. Biomechanical activation of vascular endothelium as a determinant of its functional phenotype. *Proc. Natl Acad. Sci. USA* **98,** 4478–4485 (2001).
11. Chen, X., Gays, D., Milia, C. & Santoro, M. M. Cilia control vascular mural cell recruitment in vertebrates. *Cell Reports* **18,** 1033–1047 (2017).
12. Artavanis-Tsakonas, S., Rand, M. D. & Lake, R. J. Notch signaling: cell fate control and signal integration in development. *Science* **284,** 770–776 (1999).
13. Bray, S. J. Notch signalling in context. *Nat. Rev. Mol. Cell Biol.* **17,** 722–735 (2016).
14. Weng, A. P. *et al.* Growth suppression of pre-T acute lymphoblastic leukemia cells by inhibition of Notch signaling. *Mol. Cell. Biol.* **23,** 655–664 (2003).
15. Rizzo, V., Morton, C., DePaola, N., Schnitzer, J. E. & Davies, P. F. Recruitment of endothelial caveolae into mechanotransduction pathways by flow conditioning *in vitro*. *Am. J. Physiol. Heart. Circ. Physiol.* **285,** H1720–H1729 (2003).
16. Gordon, W. R. *et al.* Mechanical allostery: evidence for a force requirement in the proteolytic activation of Notch. *Dev. Cell* **33,** 729–736 (2015).
17. Mammoto, T. *et al.* Angiopoietin-1 requires p190 RHOGAP to protect against vascular leakage *in vivo*. *J. Biol. Chem.* **282,** 23910–23918 (2007).
18. Mumm, J. S. *et al.* A ligand-induced extracellular cleavage regulates γ-secretase-like proteolytic activation of *NOTCH1*. *Mol. Cell* **5,** 197–206 (2000).
19. Huppert, S. S. *et al.* Embryonic lethality in mice homozygous for a processing-deficient allele of *Notch1*. *Nature* **405,** 966–970 (2000).
20. Spindler, V., Schlegel, N. & Waschke, J. Role of GTPases in control of microvascular permeability. *Cardiovasc. Res.* **87,** 243–253 (2010).
21. Timmerman, I. *et al.* A local VE-cadherin and TRIO-based signaling complex stabilizes endothelial junctions through RAC1. *J. Cell Sci.* **128,** 3041–3054 (2015).
22. Debant, A. *et al.* The multidomain protein TRIO binds the LAR transmembrane tyrosine phosphatase, contains a protein kinase domain, and has separate RAC-specific and RHO-specific guanine nucleotide exchange factor domains. *Proc. Natl Acad. Sci. USA* **93,** 5466–5471 (1996).
23. Le Gall, M., De Mattei, C. & Giniger, E. Molecular separation of two signaling pathways for the receptor, Notch. *Dev. Biol.* **313,** 556–567 (2008).
24. Roux, K. J., Kim, D. I., Raida, M. & Burke, B. A promiscuous biotin ligase fusion protein identifies proximal and interacting proteins in mammalian cells. *J. Cell Biol.* **196,** 801–810 (2012).
25. Coon, B. G. *et al.* Intramembrane binding of VE-cadherin to VEGFR2 and VEGFR3 assembles the endothelial mechanosensory complex. *J. Cell Biol.* **208,** 975–986 (2015).
26. Stittrich, A. B. *et al.* Mutations in *NOTCH1* cause Adams-Oliver syndrome. *Am. J. Hum. Genet.* **95,** 275–284 (2014).
27. McDaniell, R. *et al. NOTCH2* mutations cause Alagille syndrome, a heterogeneous disorder of the notch signaling pathway. *Am. J. Hum. Genet.* **79,** 169–173 (2006).
28. Joutel, A. *et al. NOTCH3* mutations in CADASIL, a hereditary adult-onset condition causing stroke and dementia. *Nature* **383,** 707–710 (1996).
29. Smith, D. C. *et al.* A phase I dose escalation and expansion study of the anticancer stem cell agent demcizumab (anti-DLL4) in patients with previously treated solid tumors. *Clin. Cancer Res.* **20,** 6295–6303 (2014).
30. Bentley, K. *et al.* The role of differential VE-cadherin dynamics in cell rearrangement during angiogenesis. *Nat. Cell Biol.* **16,** 309–321 (2014).

Supplementary Information is available in the online version of the paper.

Acknowledgements This work was supported in part by grants from the National Institutes of Health (EB00262, EB08396, UH3EB017103 and HL115553) and the National Science Foundation Center for Engineering MechanoBiology (CMMI15-48571). W.J.P. acknowledges support from a Ruth L. Kirchstein National Research Service Award (F32 HL129733) and from the NIH through the Organ Design and Engineering Training program (T32 EB16652), and M.L.K. acknowledges support from the Hartwell Foundation and the NIH through the Translational Research in Regenerative Medicine Training program (T32 EB005583). We thank P. A. Murphy and R. Wang for discussions of preliminary data and M. Schwartz for materials and discussions.

Author Contributions W.J.P., M.L.K., and C.S.C. conceived the study and designed experiments. W.J.P. and M.L.K. performed all experiments and data analysis with assistance from J.E. (qPCR) and J.Y. (*Notch1*-knockout mice). Y.W., H.V. and K.K.H. provided *Notch1*-knockout mice. W.J.P., M.L.K. and C.S.C. wrote the manuscript with input from all authors.

Author Information Reprints and permissions information is available at www.nature.com/reprints. The authors declare no competing financial interests. Readers are welcome to comment on the online version of the paper. Publisher's note: Springer Nature remains neutral with regard to jurisdictional claims in published maps and institutional affiliations. Correspondence and requests for materials should be addressed to C.S.C. (cschen@bu.edu).

Reviewer Information *Nature* thanks H. Gerhardt, I. Geudens, E. Tzima, A. Yap, and the other anonymous reviewer(s) for their contribution to the peer review of this work.

METHODS

Cell culture. Human dermal microvascular endothelial cells (hMVEC-Ds, Lonza) were maintained in EGM2-MV growth medium (Lonza) and used at passages 2–10. Human HEK293T cells (Clonetech) were cultured in DMEM (Hyclone) supplemented with 10% fetal bovine serum (Hyclone), 100 U ml^{-1} penicillin, 100 μg ml^{-1} streptomycin (Life Technologies) and 2 mM L-glutamine (Life Technologies). Both cell types were maintained at 37 °C in 5% CO_2 in a humidified incubator. Cell-line authentication (performance, differentiation, and STR profiling) was provided by Lonza and Clontech. Mycoplasma testing was performed on all lines using the PlasmoTest mycoplasma detection kit from InvivoGen.

Microfluidics. Microfluidic devices were fabricated using soft lithography. Polydimethylsiloxane (PDMS, Sylgard 184, Dow-Corning) was mixed at a ratio of 10:1 (base:curing agent) and cured overnight at 60 °C on a silicon master. The PDMS was cut from the silicon master, trimmed, and surface-activated by plasma treatment for 1 min. Devices were then bonded to glass and treated with 0.01% poly-L-lysine and 1% glutaraldehyde, washed in sterile water overnight, and sterilized with 70% ethanol for 30 min. Steel acupuncture needles (160 μm diameter, Seirin) were introduced into each device, and the devices were UV-sterilized for 20 min. Collagen type I (Thermo Fisher scientific) solution was buffered with 10× DMEM, titrated to a pH of 8.0 with NaOH, and brought to a final concentration of 2.5 mg ml^{-1} collagen I. The collagen solution was injected into the microfluidic devices and polymerized for 20 min at 37 °C. Growth medium was then added to the devices overnight and the needles were removed to create 160 μm-diameter channels in the collagen gel. hMVECs were harvested with 0.05% Trypsin-EDTA and centrifuged at 200*g* for 5 min. Cells were resuspended at 0.5 × 10^6 cells ml^{-1} in EGM2-MV, 70 μl of cell suspension was introduced into the devices and cells were allowed to adhere to collagen for 15 min before washing with growth medium. To coat collagen with DLL4, 100 μl of 1 μg ml^{-1} recombinant human DLL4 (R&D Systems) in PBS was introduced into devices and incubated on a rocker at 37 °C overnight. Devices were washed two times with PBS before seeding with cells.

To quantify vascular permeability in the microfluidic device, fluorescent dextran (70 kDa Texas Red or 70 kDa Oregon Green, Thermo Fisher) was introduced into perfusion medium at a concentration of 12.5 μg ml^{-1}, and diffusion of the dextran was imaged in real time with a Yokogawa CSU-21–Zeiss Axiovert 200M inverted spinning-disk microscope with a 10× air objective and an Evolve EMCCD camera (Photometrics). Time-lapse microscopy was used to measure the flux of dextran into the collagen gel, and the resulting diffusion profile was fitted to a dynamic mass-conservation equation as previously described[31], with the diffusive-permeability coefficient (P_D) defined by $J = P_D(c_{vessel} - c_{ECM})$, where J is the mass flux of dextran, c_{vessel} is the concentration of dextran in the vessel, and c_{ECM} is the concentration of dextran in the perivascular ECM.

To measure the effects of known permeability-inducing factors, flow imparting 5 dyn cm^{-2} wall shear stress was applied overnight and either VEGF (40 ng ml^{-1}, 1 h before permeability assay; R&D Systems) or thrombin (1 U ml^{-1}, 15 min before permeability assay; Sigma) was added. For barrier-enhancing factors, devices were left under static conditions overnight in growth medium, which was supplemented with 10 μM SU-5416 (Cayman Chemical) or 500 nM S1P (Cayman Chemical) 1 h before the permeability assay. To inhibit endocytosis in the presence of flow, devices were incubated in static conditions in medium supplemented with 60 μM Dynasore hydrate (Sigma) for 30 min before applying flow at 5 dyn cm^{-2} overnight in medium supplemented with 60 μM Dynasore.

Measurement of vascular permeability in vivo. All *in vivo* animal studies were reviewed and approved by the Institutional Animal Care and Use Committees of Boston University and Yale University. Mice were bred and maintained under specific-pathogen-free conditions at the AAALAC (Association for Assessment and Accreditation of Laboratory Animal Care International)-accredited Boston University and Yale University facilities, and housed in accordance with the procedures outlined in the Guide for the Care and Use of Laboratory Animals. For intravital measurements of vascular permeability, mice (six-to-eight-week-old female BALB/c nude mice, CrTac:NCr-*Foxn1*^{nu} strain) were anaesthetized using an isoflurane nebulizer, injected retro-orbitally with 100 μl Evans blue dye (10 mg ml^{-1} in saline) containing either DMSO or DAPT (20 μM), and immobilized on a microscope stage in an imaging chamber equilibrated to 37 °C (Extended Data Fig. 10a). Vascular-permeability images were acquired with a Leica HC FLUOTAR L 25×/0.95 W immersion objective on an upright Leica TCS SP8 multiphoton microscope equipped with a Spectra-Physics Insight DS+ laser tuned to 950 nm excitation and non-descanned emission detection at 680 nm. Vascular permeability was assessed from 20 min post-injection at 5 min intervals until 1 h post-injection. P_D was measured for five vessels per field of view as described above.

For bulk-tissue vascular-permeability measurements, inducible *NOTCH1* endothelial cell knockout mice (*Cdh5-cre*$^{ErT2+}$:*Notch1*$^{fl/fl}$) were used and their littermates (*Cdh5-cre*$^{ErT2-}$:*Notch1*$^{fl/fl}$) were used as controls. Cre was induced by injecting four-week-old mice intraperitoneally with tamoxifen (0.2 mg day^{-1}) for five consecutive days. Two weeks after the start of Cre induction, 100 μl Evans blue dye (10 mg ml^{-1} in saline) was injected retro-orbitally. Thirty minutes post-injection, animals were euthanized by cervical dislocation under anaesthesia, and blood and tissue samples were harvested, including the lungs. Blood samples were clarified at 14,000 r.p.m. for 5 min at 4 °C; freeze-dried lung samples were weighed and incubated with 500 μl formamide at 56 °C for 48 h and clarified by centrifugation. Optical density was measured at 620 nm (for Evans blue) and 740 nm (haem) using a SpectraMax M5 spectrophotometer (Molecular Devices), and the concentrations of Evans blue were calculated using the standard curve of serial dilutions of Evans blue in formamide. Levels of Evans blue in tissues were normalized by tissue weight and concentration of Evans blue in blood, and corrected for haem pigment contamination.

Antibodies and reagents. Antibodies against TRIO (H-120, 1:500), NOTCH1 ICD (C-20-R, 1:1000), NOTCH1 ECD (H-131, 1:500), VE-cadherin (F-8, 1:200) and VE-PTP (H-300, 1:250) were from Santa Cruz Biotechnology. Antibodies against VE-cadherin (ab33168, 1:2,000), RFP (ab124754, 1:1000) and β-tubulin (ab6046, 1:5,000) were from Abcam. Antibodies against VEGFR2 (55B11, 1:1000), NOTCH1 V1754G (D3B8, 1:1000 WB) and haemagglutinin (6E2, 1:1000 WB, AF647 conjugate IF) were from Cell Signaling Technologies. RAC1 antibody (102, 1:1,000) was from BD Biosciences. Rhodamine and Alexa Fluor 488-labelled phalloidin, and Alexa Fluor 488, 568 and 647 goat anti-mouse and anti-rabbit IgG secondary antibodies were from Life Technologies. HRP-conjugated donkey anti-mouse, anti-rabbit, and anti-goat IgG secondary antibodies were from Fitzgerald. PTPRF antibody (SAB4200321, 1:1,000), DAPI, DAPT, Evans blue dye, and formamide were from Sigma. The RAC1 inhibitor NSC 23766 was from Santa Cruz Biotechnology.

Cloning and qPCR. Human *CDH5* (gift from M. Davidson) and human *NOTCH1* (gift from M. Elowitz) cDNAs were used to make C-terminal mApple-tagged constructs in a modified pRRL lentiviral expression vector. PCR amplification of the following amino acid sites was used to make C-terminal mApple-tagged NOTCH1 truncation constructs: TMD–ICD–mApple (S2 cleavage site to end of ICD, Val1721–Lys2555) and TMD–mApple (S2 to S3 cleavage site, Val1721–Gly1753). The DN-MAML construct (MSCV-IRES–GFP MAML1 13–74) was from J. Aster. Human *DLL4* cDNA (Sino Biological) was modified with an N-terminal haemagglutinin tag by PCR and cloned into a modified pRRL lentiviral expression vector. All constructs were expressed by lentiviral transduction.

Endothelial cells were lysed with Trizol (LifeTechnologies) followed by chloroform phase separation. The aqueous phase was diluted with 70% ethanol at a 1:1 ratio, loaded on an RNA micro column (RNA microkit, Qiagen SciencesSA) and RNA extraction was performed according to the manufacturer's protocol. Subsequently, 1 μg total RNA was converted to cDNA with qScript cDNA Supermix (Quanta Sciences). Real-time PCR was performed in 20-μl reactions using the SYBR Green Mastermix I (Roche) and a LightCycler480 (Roche), with 40 cycles of 95 °C for 3 s, 60 °C for 10 s and 72 °C for 20 s. Specific gene targets were detected with the primers listed in Supplementary Table 1. Primers for *NOTCH1* and *DLL1* were acquired from Qiagen (Quantitec Hs_NOTCH1_2_SG, Quanititec Hs_DLL1_1_SG).

Relative gene expression is expressed as $-\Delta\Delta C_t$, in which ΔC_t is the difference in C_t value between the gene of interest (GOI) and a housekeeping gene (proteasome subunit beta type-2 (*PSMB2*) or glyceraldehyde 3-phosphate dehydrogenase (*GAPDH*)) and $\Delta\Delta C_t$ is the difference between the ΔC_t of the GOI in an experimental condition and the ΔC_t of the same GOI in a control condition. Heat maps showing $-\Delta\Delta C_t$ of the GOI under flow normalized to static controls were generated using Genesis v1.8.1[32]. Primer sequences for qPCR are shown in Supplementary Table 1.

Lentiviral-mediated CRISPR genome editing. Stable CRISPR-knockout primary hMVEC-D cell lines in were generated using the lentiCRISPRv2 system (gift from F. Zhang, Addgene plasmid #52961). Specific guide (g)RNAs were generated using the Optimized CRISPR Design tool (F. Zhang) and cloned into the BsmBI site of plentiCRISPRv2. gRNAs used for both silencing and truncation of genomic targets are summarized in Supplementary Table 2. Individual gRNA-containing plentiCRISPRv2 plasmids were co-transfected with pVSVG, pRSV-REV, and pMDLg/pRRE packaging plasmids into HEK-293T cells using calcium phosphate transfection. After 48 h, viral supernatants were collected, concentrated using PEG-IT viral precipitator (SBI), and resuspended in PBS. hMVEC-Ds were transduced in growth medium overnight and medium was replaced the following morning. At 48 h after infection, cells were plated in 6-well plates at 75,000 cells per well and selected with 2 μg ml^{-1} puromycin for 3–4 days. All CRISPR modifications were verified by western blot.

GTPase activity assays. The pGEX4T-1 construct containing the p21-binding domain of PAK1 (PBD) was from Addgene (Plasmid 12217). In brief, expression

of the GST fusion protein in BL21 *Escherichia coli* was induced with 200 μM isopropyl-β-D-thiogalactoside (IPTG) for 12–16 h at room temperature. Bacterial cells were lysed in buffer containing 25 mM HEPES pH 7.6, 1% Triton X-100, 150 mM NaCl, 5 mM $MgCl_2$, 1 mM dithiothreitol, and protease and phosphatase inhibitor cocktails (Roche), and the proteins were purified by incubation with glutathione–Sepharose 4B beads (GE Healthcare) at 4 °C. For active RAC1 pull-downs, confluent hMVEC-Ds plated on 50 μg ml^{-1} collagen I in reduced serum growth medium (0.5% FBS) were rinsed with cold PBS containing 1 mM Ca^{2+} and 0.5 mM Mg^{2+} (PBS+), then lysed with cold 50 mM Tris pH 7.6, 200 mM NaCl, 1% Triton X-100, 0.5% deoxycholate, 5 mM $MgCl_2$, and protease and phosphatase inhibitor cocktails, sonicated at 3 W on ice for 5 s, and clarified at 14,000*g* for 5 min. Lysates were equalized for protein content and volume and rotated at 4 °C for 1 h with 20 μg GST–PBD. Bead pellets were washed three times with lysis buffer, extracted in 2× NuPAGE LDS sample buffer (Life Technologies) containing 100 mM DTT, and analysed by SDS–PAGE and immunoblotting with chemiluminescent HRP detection. Western blots were adjusted for brightness and contrast using ImageJ. Active RAC1 quantifications were normalized to total RAC1 for each condition.

Immunoprecipitation. Confluent hMVEC-Ds plated on 50 μg ml^{-1} collagen I and cultured in growth medium were rinsed with cold PBS+, then lysed with cold 25 mM HEPES, pH 7.5, 200 mM NaCl, 1% Triton X-100, 5 mM $MgCl_2$, and 1.5× protease and phosphatase inhibitors (Roche). Lysates were drawn through a 21G syringe 15 times and incubated on ice for 30 min before clarification at 14,000*g* for 15 min at 4 °C. Clarified lysates were equalized for protein content and volume and incubated with 2 μg of anti-VE-cadherin, 2 μg of anti-TRIO, or 2 μg anti-NOTCH1 antibodies at 4 °C with end-over-end rotation. Antibody complexes were purified with Protein A/G beads (Life Technologies) at 4 °C with end-over-end rotation. Bead pellets were washed three times with lysis buffer. Protein complexes were extracted in 2× NuPAGE LDS Sample Buffer (Life Technologies) containing 100 mM DTT and analysed by SDS–PAGE and immunoblotting with chemiluminescent HRP detection. Western blots were adjusted for brightness and contrast using ImageJ.

For immunoprecipitation of VE-cadherin and Trio from mouse lung lysates, age and sex-matched *Cdh5-cre^{ErT2-}:Notch1$^{fl/fl}$* and *Cdh5-cre^{ErT2+}:Notch1$^{fl/fl}$* littermates were euthanized by cervical dislocation under anaesthesia and lungs were removed and immediately snap frozen in liquid nitrogen. Mouse lungs were homogenized in a Potter-Elvehjem tissue grinder in lysis buffer (25 mM HEPES pH 7.5, 1 mM EDTA, 150 mM NaCl, 0.5% Triton X-100, 0.5% NP-40, and 1.5× protease and phosphatase inhibitor cocktail (ThermoFisher)), and clarified by centrifugation at 20,000*g* for 30 min at 4 °C. The soluble supernatants were pre-cleared with protein-G sepharose beads and then incubated with protein-G sepharose beads with VE-cadherin or Trio antibody (Santa Cruz, 1 mg) for 3 h at 4 °C, washed three times with lysis buffer and then processed in SDS–PAGE sample buffer.

Immunofluorescence. For morphological analysis of adherens junctions and actin cytoskeleton, cells cultured in complete medium were permeabilized and fixed with 1% paraformaldehyde, 0.03% Triton X-100 in PBS+ at 37 °C for 90 s, and immediately post-fixed in 4% paraformaldehyde in PBS+ at 37 °C for 15 min. The cells were rinsed three times with PBS+ and permeabilized with 0.5% Triton X-100 in PBS+ for 10 min. Cells were blocked with 2% BSA in PBS+. Primary and secondary antibodies were applied in 2% BSA in PBS+ and rinsed three times over 30 min with PBS+ between each treatment. To examine the localization of endogenous NOTCH1 and TMD–mApple, cells cultured in complete medium were fixed with 4% paraformaldehyde in PBS+, permeabilized with 0.1% Triton X-100 in PBS+, and blocked with 2% BSA in PBS+. Primary and secondary antibodies were applied in 2% BSA in PBS+ and rinsed three times over 30 min with PBS+ between each treatment. For live-cell or immunofluorescent imaging, images were acquired with a Yokogawa CSU-21/Zeiss Axiovert 200M inverted spinning disk microscope with either a Zeiss LD C-Apochromat 40×, 1.1 N.A. or 63×, 1.15 N.A. water-immersion objective and an Evolve EMCCD camera (Photometrics). Fluorescence images were adjusted for brightness and contrast using ImageJ and MATLAB software.

To quantify junctional organization, greyscale micrographs of cells immunostained for VE-cadherin were converted to black and white based on a threshold determined by Otsu's method, and junctional area was defined as the total number of pixels above the threshold. To quantify actin stress fibres and cortical actin, the intensity of Alexa Fluor 488 phalloidin-labelled cells was plotted along lines drawn between the centroids in the nuclei of neighbouring cells. Local intensity peaks were measured to determine stress fibre locations (Extended Data Fig. 10b). Cortical actin was defined as the area under the peak at cell–cell junctions normalized to total area under the curve, and stress fibres were quantified as the number of peaks normalized by the total length of the line between nucleus centroids.

To measure DLL4 endocytosis, endothelial cells expressing haemagglutinin (HA)-tagged DLL4 (DLL4–HA) were seeded into flow chambers (Ibidi) and cultured for 6 h under static conditions. Dynasore hydrate or DMSO-load control was added for 30 min, followed by AlexaFluor 488-conjugated mouse heamagglutinin antibody (1:250) in medium containing Dynasore or DMSO for 30 min before washing with medium containing Dynasore or DMSO. Devices were then cultured in static conditions or under flow imparting 5 dyn cm^{-2} shear stress for 1 h in medium containing Dynasore or DMSO before fixation with 4% PFA in PBS+ at 37 °C for 15 min. Cells were permeabilized with 0.025% saponin (Sigma) and 2% BSA in PBS+ for 30 min at room temperature, and all subsequent antibody incubations and washes were performed in this buffer. Cells were incubated with anti-NOTCH1 ECD rabbit antibody (1:200) overnight at room temperature before AlexaFluor 488 anti-mouse (1:200) and AlexaFluor 568 anti-rabbit (1:200) antibodies were added for 2 h at 4 °C. The fraction of cells with internalized DLL4 was determined by counting the number of cells with more than one haemagglutinin-positive punctum and the total number of cells labelled by DAPI staining.

Statistical analysis. Sample sizes and *P* values are reported in the figure legends and statistical analyses were performed using GraphPad Prism 6.0 or Microsoft Excel. Unless otherwise noted in the figure legend, statistical differences between sets of data were analysed with a two-tailed, unpaired Student's *t*-test, and exact *P* values are provided in the Source Data. Sample sizes of sufficient power were chosen on the basis of similar published research and were confirmed statistically by appropriate tests. Experiments were not randomized and experimenters were not blinded to experimental conditions.

Data availability. Graphical Source Data are provided for each figure. The source images for the western blots in the figures are available in the Supplementary Information. Additional data that support the findings of this study are available from the corresponding author upon reasonable request.

31. Adamson, R. H., Lenz, J. F. & Curry, F. E. Quantitative laser scanning confocal microscopy on single capillaries: permeability measurement. *Microcirculation* **1,** 251–265 (1994).
32. Sturn, A., Quackenbush, J. & Trajanoski, Z. Genesis: cluster analysis of microarray data. *Bioinformatics* **18,** 207–208 (2002).

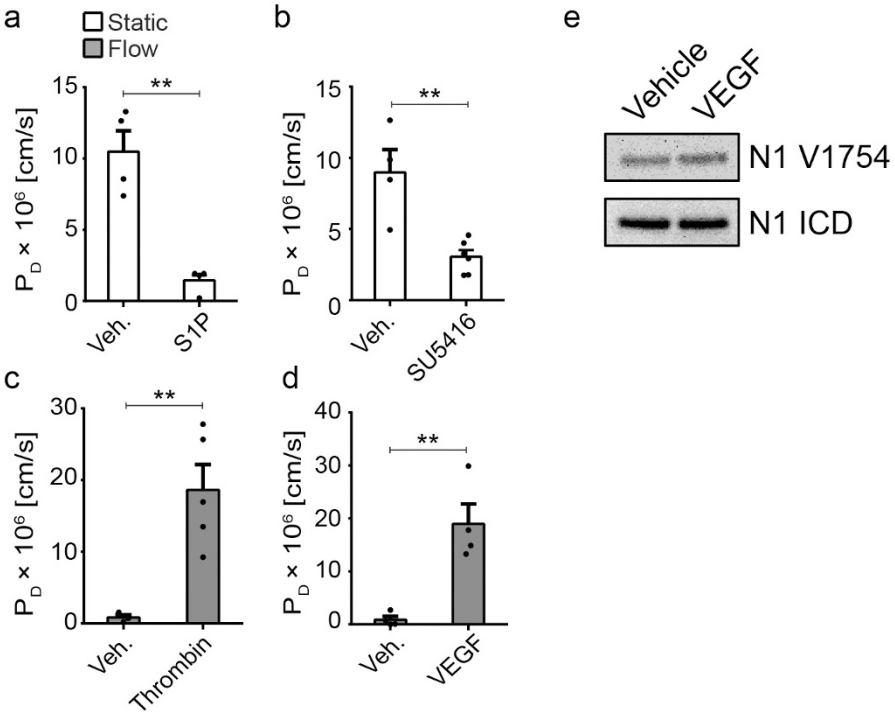

Extended Data Figure 1 | Known permeability-modulating agents regulate barrier function in hEMVs. a–d, Diffusive permeability measured in hEMVs in static or flow conditions treated with 500 nM S1P for 1 h (**a**), 10 μM SU415 (VEGFR2 inhibitor) overnight (**b**), 1 U ml^{-1} thrombin for 15 min (**c**), or 40 ng ml^{-1} VEGF for 1 h (**d**). **e**, Western blots of cleaved NOTCH1 ICD (using N1 V1754 antibody) from lysates of endothelial cells treated with vehicle or 40 ng ml^{-1} VEGF for 1 h. All plots show mean ± s.e.m., $n \geq 3$ hEMVs, $^{**}P < 0.01$. Exact *P* and *n* values are shown in Source Data; western blot is representative of two independent experiments.

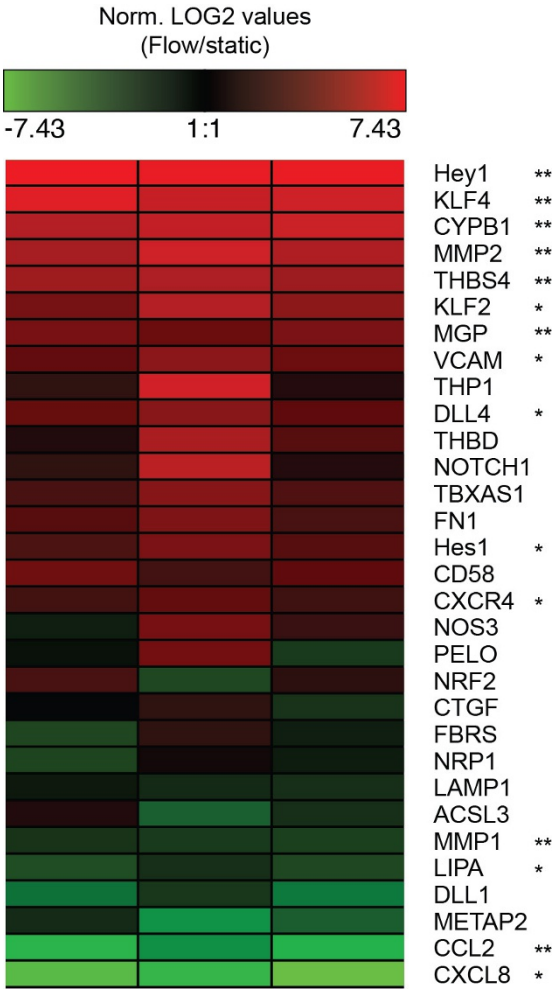

Extended Data Figure 2 | Flow activates expression of mechanotransduction-associated gene networks. Relative gene expression measured by qPCR. $-\Delta\Delta C_t$ of GOI under flow normalized to static control is plotted as a heat map ($n = 3$ flow or static qPCR analyses from distinct hEMV sets; each column is representative of an independent experiment; $^*P < 0.05$, $^{**}P < 0.01$). Exact P and n values are shown in Source Data.

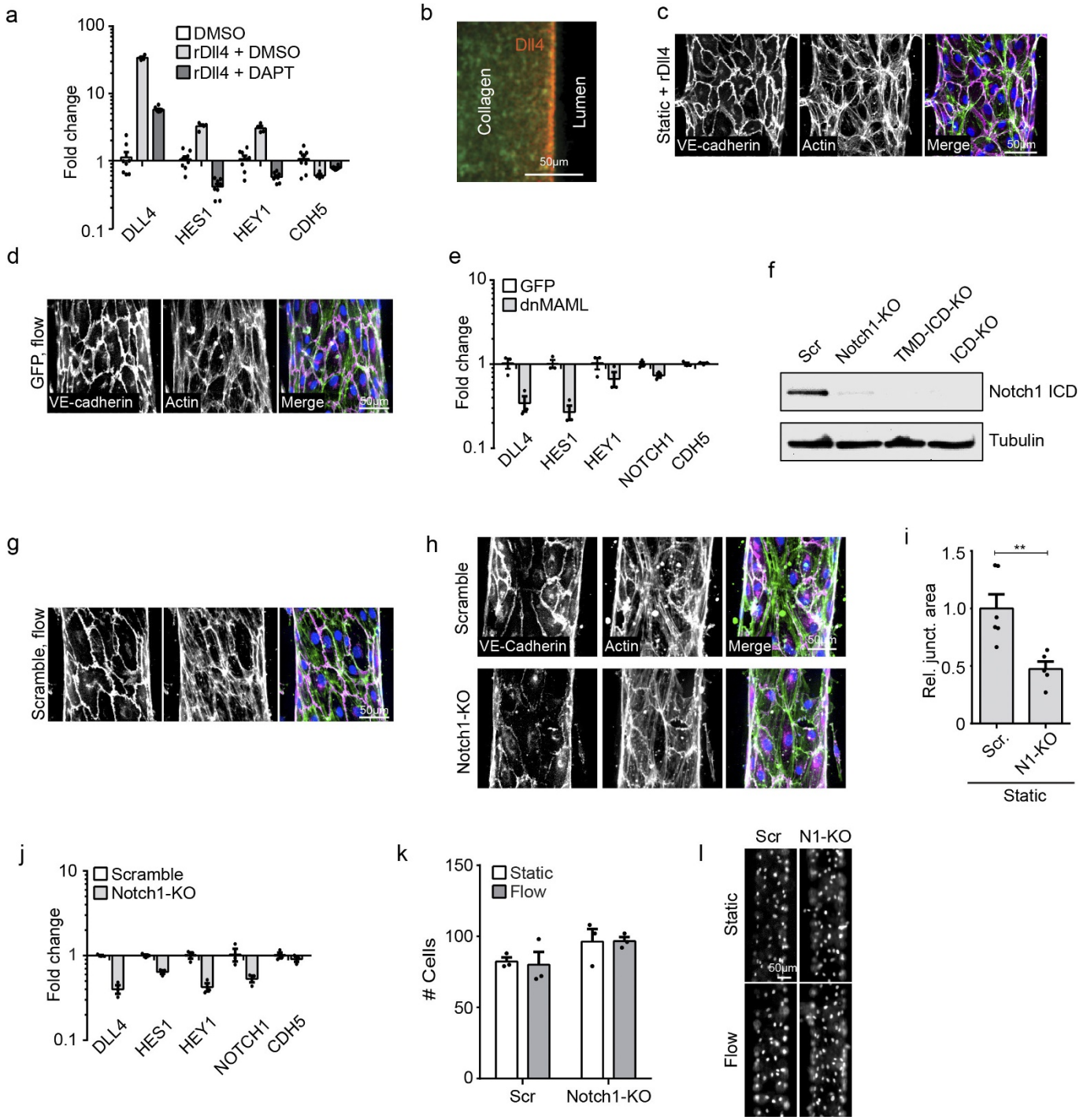

Extended Data Figure 3 | Non-transcriptional NOTCH1 signalling regulates vascular barrier function. a, Expression of NOTCH1-target genes *HES1* and *HEY1* and the genes for the NOTCH1 ligand (*DLL4*) and VE-cadherin (*CDH5*) measured by qPCR in endothelial cells treated with DAPT or DMSO-load control on DLL4-coated and control tissue culture plastic substrates. **b**, Fluorescent micrograph of DLL4-coated device before cell seeding (green, Alexa Fluor 488–collagen I; red, DLL4 immunofluorescence). **c**, Fluorescent micrograph of endothelial cells in hEMVs coated with DLL4 before cell seeding. **d**, Micrographs of GFP-infection control cells under flow. **e**, Gene expression of *HES1*, *HEY1*, *DLL4*, *NOTCH1*, and *CDH5* measured by qPCR in endothelial cells expressing dominant-negative MAML (dnMAML) or infection control (GFP). **f**, Western blot validation of NOTCH1 CRISPR lines: Scramble, $NOTCH1^{KO}$, TMD-ICD KO, and ICD KO. **g**, Fluorescent micrographs of CRISPR–Cas9 scramble control cells cultured in flow conditions. **h**, Fluorescent micrographs of scramble control and $NOTCH1^{KO}$ hEMVs cultured in static conditions, immunostained for VE-cadherin and labelled with phalloidin. **i**, Quantification of junctional area measured from micrographs of cells immunostained for VE-cadherin as described in **h**. **j**, Gene expression measured by qPCR in $NOTCH1^{KO}$ and scramble control cells. **k**, Quantification of cell number in field of view at 10× magnification of scramble or $NOTCH1^{KO}$ hEMVs cultured in static and flow conditions. **l**, Micrographs of nuclei as visualized by DAPI in scramble or $NOTCH1^{KO}$ hEMVs. For all plots, mean ± s.e.m., $n \geq 3$ hEMVs, $^{**}P < 0.01$. Exact *P* and *n* values are shown in Source Data; images are representative of at least three independent experiments.

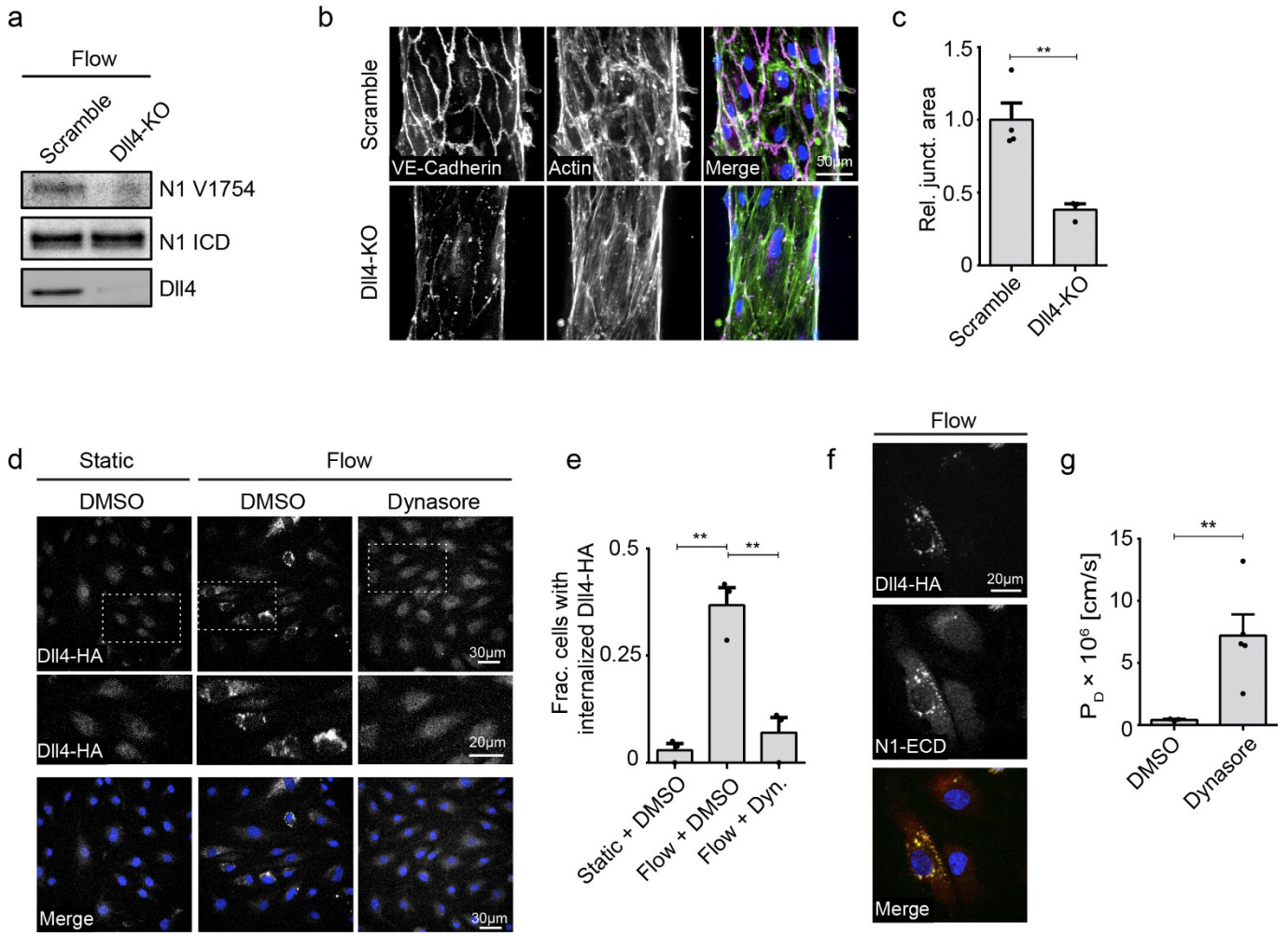

Extended Data Figure 4 | NOTCH1 is activated in response to shear stress by endocytosis of DLL4. a, ICD cleavage as measured by western blot with an antibody specific to cleaved ICD (N1 V1754) in *DLL4*^{KO} and scramble control endothelial cells cultured under flow. **b**, Fluorescent micrographs of *DLL4*^{KO} and scramble control hEMVs cultured under flow conditions, immunostained for VE-cadherin and labelled with phalloidin. **c**, Quantification of junctional area measured from micrographs of cells immunostained for VE-cadherin. **d**, Fluorescence micrograph of endothelial cells expressing DLL4–HA in static plus DMSO, flow plus DMSO, and flow plus Dynasore conditions, stained for haemagglutinin and DAPI. **e**, Quantification of internalized DLL4–HA in endothelial cells under static plus DMSO, flow plus DMSO, and flow plus Dynasore conditions. Cells with more than one Alexa Fluor 488-positive punctum counted as positive for internalized DLL4–HA. **f**, Immunofluorescence of an endothelial cell expressing DLL4–HA cultured under flow and stained for haemagglutinin and NOTCH1 ECD and stained with DAPI. **g**, Diffusive permeability of 70-kDa dextran in cells treated with Dynasore hydrate or DMSO-load control and exposed to flow overnight. All plots show mean ± s.e.m., $n \geq 3$ hEMVs, $^{**}P < 0.01$. Exact P and n values are given in Source Data; images are representative of at least two independent experiments.

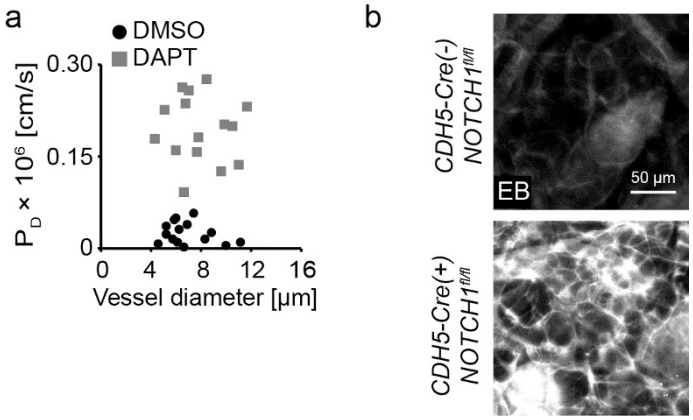

Extended Data Figure 5 | DAPT and NOTCH1 depletion modulate vascular permeability *in vivo*. a, Diffusive permeability of mouse dermal vasculature as a function of vessel diameter after 1 h of intravenously injected DMSO or DAPT ($n = 15$ vessels across 3 mice per condition). **b**, High magnification whole-mount micrographs of Evans blue in the mouse dermal vasculature. Fluorescent images are representative of three independent experiments.

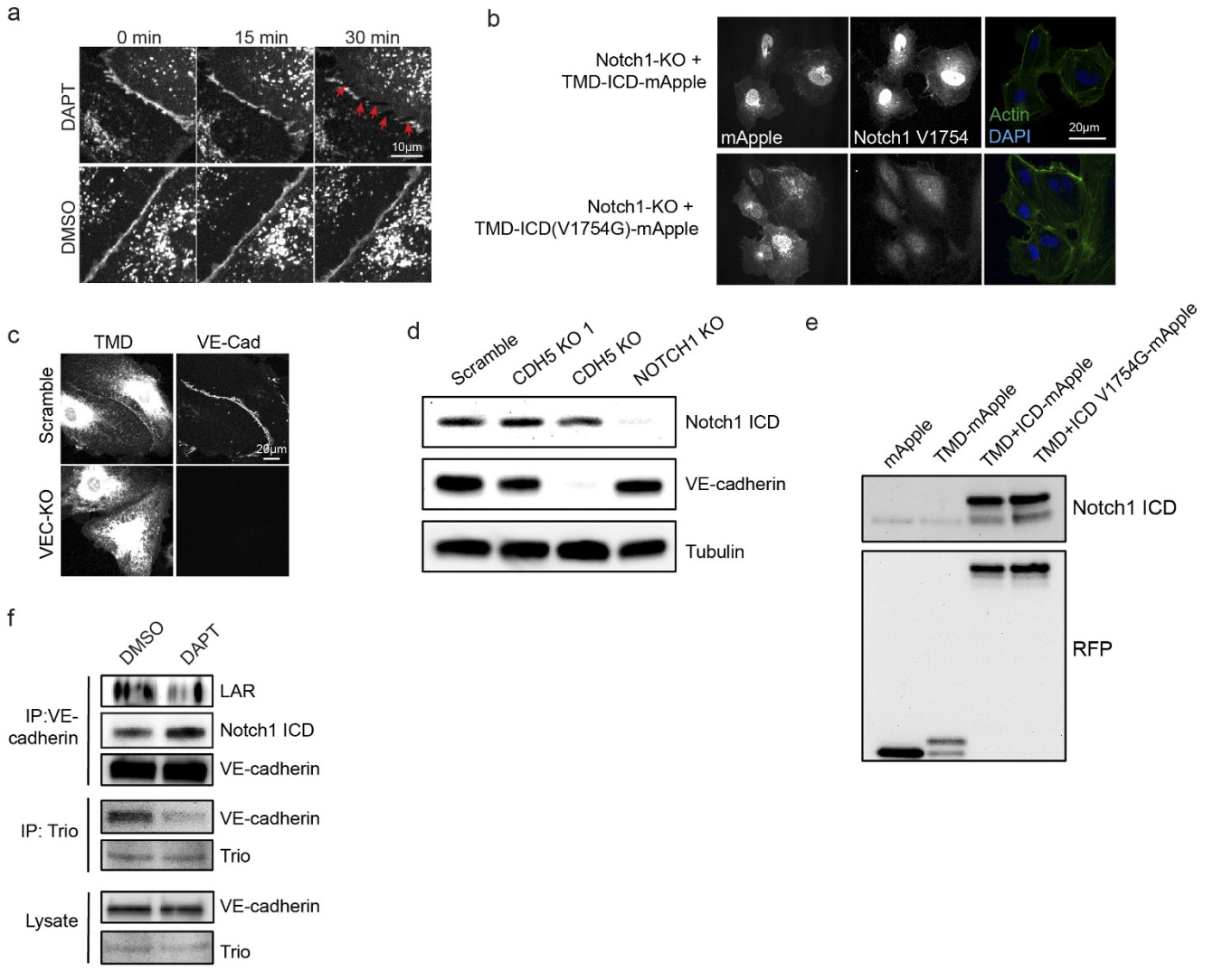

Extended Data Figure 6 | NOTCH1 regulates junctional stability through association with VE-cadherin. a, Time-lapse images of cells expressing VE-cadherin–mApple in the presence of DAPT or DMSO load control demonstrate that adherens junctions disassemble after 30 min of exposure to DAPT, leading to macroscopic intercellular gaps (red arrows). **b**, Fluorescent micrographs of *NOTCH1*^{KO} cells expressing TMD–ICD–mApple or TMD–ICD(V1754G)–mApple immunostained for cleaved NOTCH1 (ICD V1754) and stained with DAPI. **c**, Fluorescent micrographs of TMD–mApple expressed in *CHD5*^{KO} or scramble control endothelial cells and immunostained for VE-cadherin. **d**, Western blot for NOTCH1 ICD and VE-cadherin in *NOTCH1*^{KO} and *CHD5*^{KO} endothelial cells. **e**, Western blot validation of NOTCH1 rescue constructs: mApple, TMD–mApple, ICD–TMD–mApple, and ICD–TMD(V1754G)–mApple. **f**, Immunoprecipitation of VE-cadherin from hMVEC-D cells treated with DMSO or DAPT. Co-immunoprecipitation of mechanosensory complex components was assessed by immunoblotting for NOTCH1 ICD, TRIO, and LAR. **g**. Western blot of VE-cadherin immunoprecipitations from *NOTCH1*^{KO} cells expressing NOTCH1-TMD truncation constructs (6, 8 and 12 amino acids from the N terminus) fused to mApple. **h**, Western blot of VE-cadherin immunoprecipitations from *NOTCH1*^{KO} cells expressing NOTCH1 TMD constructs with single and double point mutations within the TMD and fused to mApple. Images are representative of at least three independent experiments.

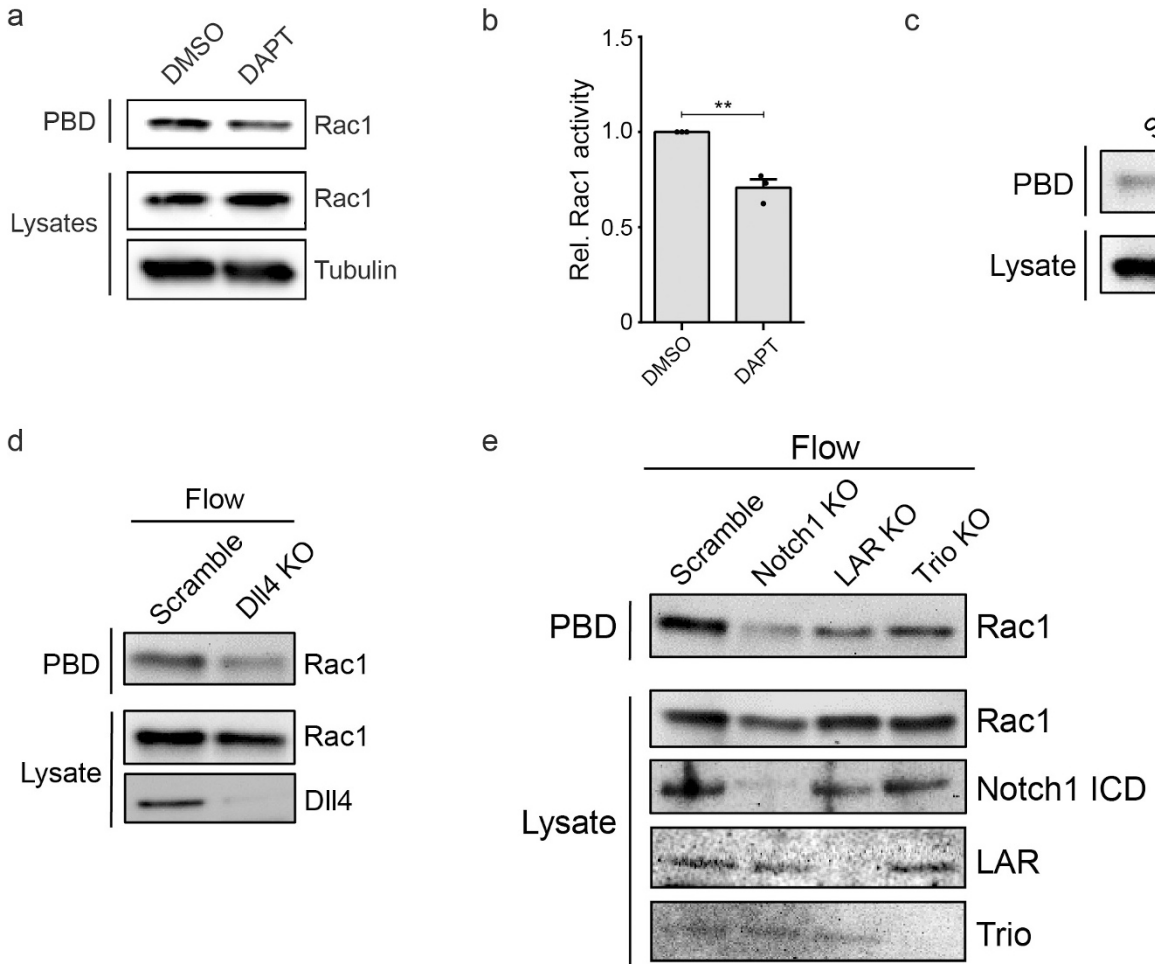

Extended Data Figure 7 | DLL4 and the NOTCH1 mechanosensory complex are critical for increased RAC1 activity in response to shear stress. a, Active RAC1 was isolated from hMVEC-D cell lysates treated with DMSO and DAPT (20 μM) using a pull-down assay with GST–PBD. **b**, Quantification of band intensity from **a** demonstrates a decrease (∼30%) in RAC1 activity with DAPT treatment. **c**, Active RAC1 was isolated from hMVEC-D cell lysates from static or shear flow conditions using GST–PBD pull-down. **d**, Active RAC1 was isolated using GST–PBD pull-down from $DLL4^{KO}$ cell lysates under flow conditions. **e**, Active RAC1 was isolated using GST–PBD pull-down from $NOTCH1^{KO}$, $PTPRF^{KO}$ and $TRIO^{KO}$ cell lysates under flow conditions. Mean ± s.e.m., $n = 3$ independent lysates, $^{**}P < 0.01$. Exact P and n values are shown in Source Data; all images are representative of at least three independent experiments.

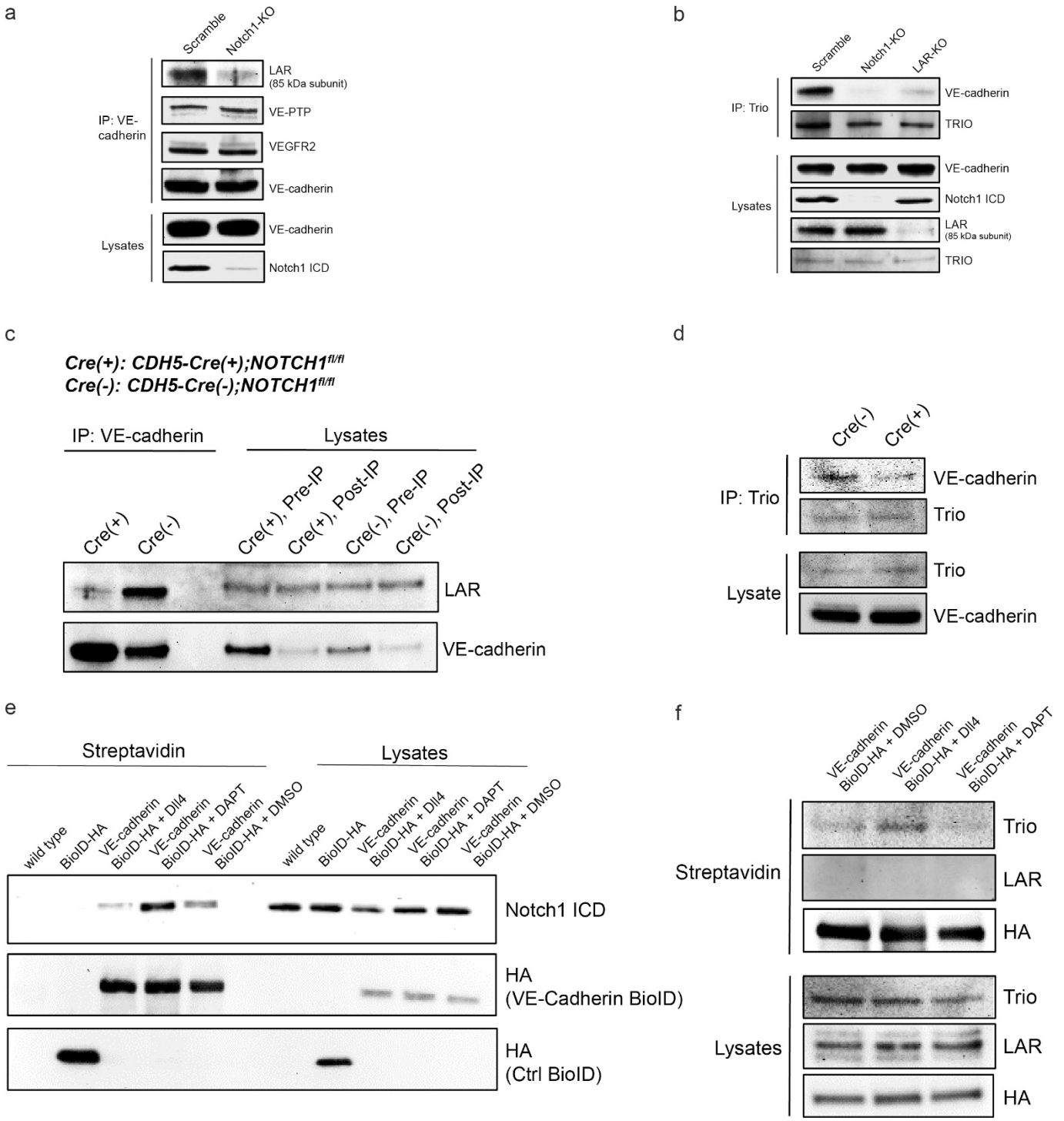

Extended Data Figure 8 | NOTCH1 regulates VE-cadherin-interacting proteins to form the NOTCH1 mechanosensory complex. **a**, Immunoprecipitation of VE-cadherin from *NOTCH1*^{KO} and scramble control cells. Co-immunoprecipitation of candidate NOTCH1-dependent VE-cadherin effectors was assessed by immunoblotting for VE-PTP, VEGFR2 and LAR (85 kDa P subunit). **b**, Immunoprecipitation of TRIO from scramble control, *NOTCH1*^{KO}, and *PTPRF*^{KO} cells. Immunoblotting for VE-cadherin was used to assess impaired TRIO–VE-cadherin co-immunoprecipitation on depletion of NOTCH1 or LAR. **c**, Western blots of VE-cadherin immunoprecipitates of lysates from lungs of *Cdh5-cre*$^{+}$*:Notch1*$^{fl/fl}$ and control *Cdh5-cre*$^{-}$*:Notch1*$^{fl/fl}$ mice. **d**, Western blots of Trio immunoprecipitates from lysates of lungs from *Cdh5-cre*$^{+}$*:Notch1*$^{fl/fl}$ and control *Cdh5-cre*$^{-}$*:Notch1*$^{fl/fl}$ mice. **e**, Western blot of proximal interacting proteins extracted with streptavidin from hMVEC-D cells expressing BIRA–HA (BioID) or VE-cadherin–BIRA–HA (VE-BioID) that were treated with DLL4, DAPT or DMSO. **f**, Western blot of proximal interacting proteins extracted with streptavidin in hMVEC-D cells expressing VE-cadherin–BIRA–HA (VE-BioID) that were treated with DLL4, DAPT or DMSO. Images are representative of at least two independent experiments.

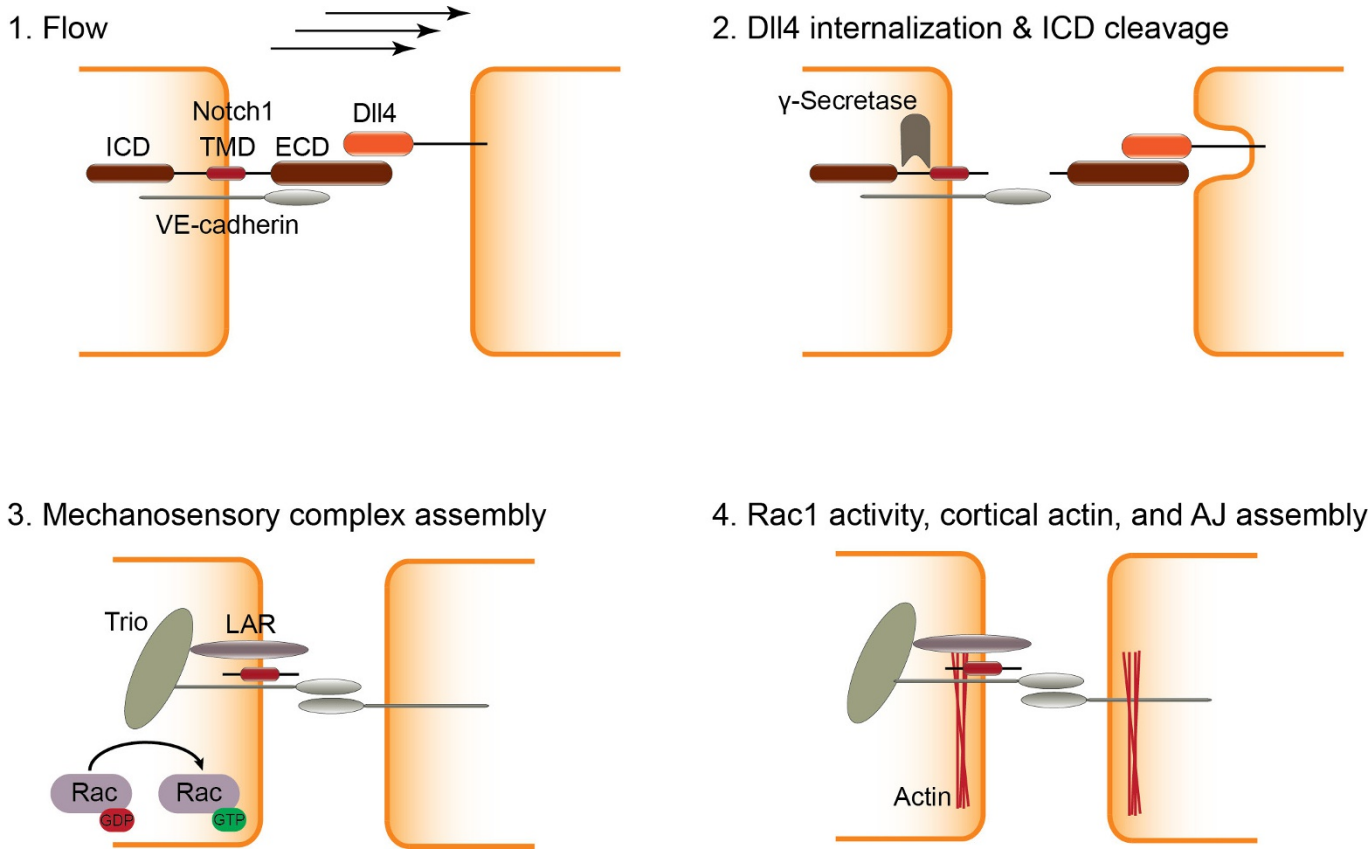

Extended Data Figure 9 | The NOTCH1 mechanosensory complex stabilizes cell–cell junctions through activation of RAC1. Flow induces endocytosis of DLL4, triggering the activation and cleavage of NOTCH1 ICD and ECD, which allows the NOTCH1 TMD to link the adaptor protein LAR with VE-cadherin and recruit TRIO to adherens junctions. The resulting complex activates RAC1, elaborates cortical actin, and stabilizes cell–cell junctions to establish barrier function.

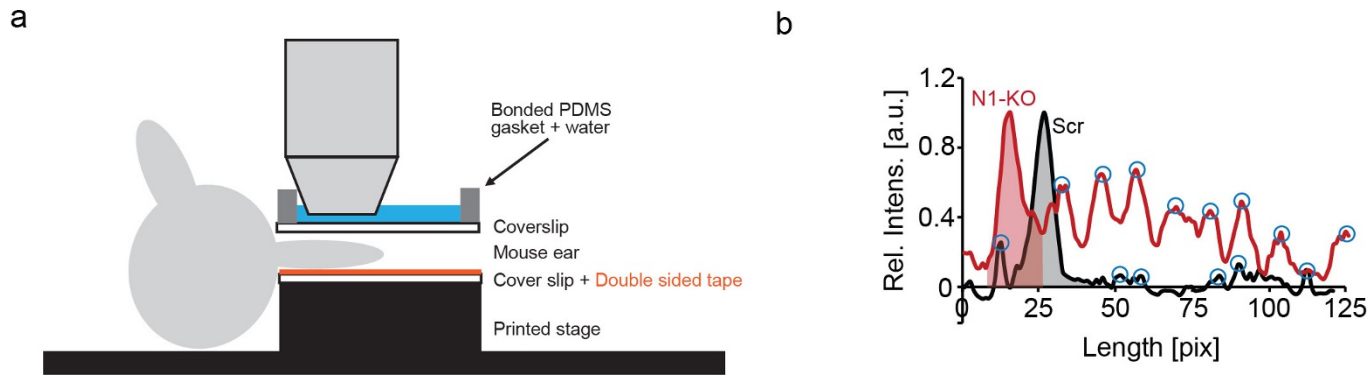

Extended Data Figure 10 | Supplementary methods. a, Schematic and summary of methods for quantifying vascular permeability *in vivo* with intravital microscopy. **b**, Intensity as a function of distance along lines connecting the nucleus centroids of neighbouring cells. Blue circles are local maxima used to count the number of stress fibres per unit length, and the shaded region is the area under the peak corresponding to cortical actin, and is normalized against the total area under the curve for quantification. The graph is representative of three independent experiments.

nature research

Corresponding author(s): Christopher Chen

☐ Initial submission ☐ Revised version ☒ Final submission

Life Sciences Reporting Summary

Nature Research wishes to improve the reproducibility of the work that we publish. This form is intended for publication with all accepted life science papers and provides structure for consistency and transparency in reporting. Every life science submission will use this form; some list items might not apply to an individual manuscript, but all fields must be completed for clarity.

For further information on the points included in this form, see Reporting Life Sciences Research. For further information on Nature Research policies, including our data availability policy, see Authors & Referees and the Editorial Policy Checklist.

Experimental design

1. Sample size

Describe how sample size was determined.

Supplemental Methods, "Statistical Analysis":
"Sample sizes of sufficient power were chosen on the basis of similar published research and were confirmed statistically by appropriate tests."

2. Data exclusions

Describe any data exclusions.

No samples or animals were excluded.

3. Replication

Describe whether the experimental findings were reliably reproduced.

All attempts at replication were successful.

4. Randomization

Describe how samples/organisms/participants were allocated into experimental groups.

Age/sex matched litter mates were assigned to groups by genotype. No randomization was used.

5. Blinding

Describe whether the investigators were blinded to group allocation during data collection and/or analysis.

No blinding.

Note: all studies involving animals and/or human research participants must disclose whether blinding and randomization were used.

6. Statistical parameters

For all figures and tables that use statistical methods, confirm that the following items are present in relevant figure legends (or in the Methods section if additional space is needed).

n/a	Confirmed	
☐	☒	The exact sample size (*n*) for each experimental group/condition, given as a discrete number and unit of measurement (animals, litters, cultures, etc.)
☐	☒	A description of how samples were collected, noting whether measurements were taken from distinct samples or whether the same sample was measured repeatedly
☐	☒	A statement indicating how many times each experiment was replicated
☐	☒	The statistical test(s) used and whether they are one- or two-sided (note: only common tests should be described solely by name; more complex techniques should be described in the Methods section)
☐	☒	A description of any assumptions or corrections, such as an adjustment for multiple comparisons
☐	☒	The test results (e.g. *P* values) given as exact values whenever possible and with confidence intervals noted
☐	☒	A clear description of statistics including central tendency (e.g. median, mean) and variation (e.g. standard deviation, interquartile range)
☐	☒	Clearly defined error bars

See the web collection on statistics for biologists for further resources and guidance.

Software

Policy information about availability of computer code

7. Software

Describe the software used to analyze the data in this study.	Data were analyzed using MATLAB R2015b, ImageJ/FIJI, and GraphPad Prism 6.

For manuscripts utilizing custom algorithms or software that are central to the paper but not yet described in the published literature, software must be made available to editors and reviewers upon request. We strongly encourage code deposition in a community repository (e.g. GitHub). *Nature Methods* guidance for providing algorithms and software for publication provides further information on this topic.

Materials and reagents

Policy information about availability of materials

8. Materials availability

Indicate whether there are restrictions on availability of unique materials or if these materials are only available for distribution by a for-profit company.	All materials are commercially available.

9. Antibodies

Describe the antibodies used and how they were validated for use in the system under study (i.e. assay and species).	All antibodies (supplier name, catalog number/clone name, dilution) are provided in the Methods section under "Antibodies and reagents" as follows: The anti-Trio (H-120, 1:500), anti-Notch1 ICD (C-20-R, 1:1000), anti-Notch1 ECD (H-131, 1:500), anti-VE-cadherin (F-8, 1:200), and anti-VE-PTP (H-300, 1:250) antibodies were from Santa Cruz Biotechnology. Anti-VE-cadherin (ab33168, 1:2,000), anti-RFP (ab124754, 1:1000), and anti-β tubulin (ab6046, 1:5,000) antibodies were from Abcam. Anti-VEGFR2 antibody (55B11, 1:1000), anti-Notch1 V1754G (D3B8, 1:1000 WB), anti-HA (6E2, 1:1000 WB, AF647 conjugate IF) was from Cell Signaling Technologies. Anti-Rac1 antibody (102, 1:1,000) was from BD Biosciences. Rhodamine and Alexa Fluor 488-labelled phalloidin, Alexa Fluor-488, 568 and 647 goat anti-mouse and anti-rabbit IgG secondary antibodies were were from Life Technologies. HRP-conjugated donkey anti-mouse, anti-rabbit, and anti-goat IgG secondary antibodies were from Fitzgerald. Anti-PTPRF antibody (SAB4200321, 1:1000), DAPI, DAPT, Evans Blue dye, dynasore hydrate, and formamide were from Sigma. Rac1 inhibitor NSC 23766 was from Santa Cruz Biotechnology. Primary antibodies were validated for use based on the position the antigen in SDS-PAGE gels, the disappearance of antigen upon CRISPR deletion, and immunofluoresence.

10. Eukaryotic cell lines

a. State the source of each eukaryotic cell line used.	The cell lines used are described in the materials and methods under "Cell culture" as follows: Human dermal microvascular endothelial cells (hMVEC-Ds, Lonza) were maintained in EGM2-MV growth media (Lonza) and used at passages 2-10. Human HEK293T (Clonetech) were cultured in DMEM (Hyclone) supplemented with 10% fetal bovine serum (Hyclone), 100 U ml−1 penicillin, 100 µg ml−1 streptomycin (Life Technologies) and 2 mM L-glutamine (Life Technologies). Both cell types were maintained at 37 °C in 5% CO2 in a humidified incubator.
b. Describe the method of cell line authentication used.	Not authenticated beyond the virus testing (HIV, HBV, HCV), microbial testing (sterility, mycoplasma), cell performance testing (viability, cell count, seeding efficiency, doubling time), and contamination/differentiation testing (CD31 and podoplanin expression) provided by Lonza quality assurance.
c. Report whether the cell lines were tested for mycoplasma contamination.	Mycoplasma testing was performed on all lines using PlasmoTest mycoplasma detection kit from InvivoGen.
d. If any of the cell lines used are listed in the database of commonly misidentified cell lines maintained by ICLAC, provide a scientific rationale for their use.	Cell lines are not listed in database of commonly misidentified cell lines.

Animals and human research participants

Policy information about studies involving animals; when reporting animal research, follow the ARRIVE guidelines

11. Description of research animals

Provide details on animals and/or animal-derived materials used in the study.

Supplemental Methods: "Measurement of vascular permeability in vivo"
All in vivo animal studies were reviewed and approved by the institutional animal care and use committees of Boston University and Yale University. For intravital measurements of vascular permeability, mice (6-8 weeks old, BALB/c nude mice CrTac:NCr-Foxn1nu strain, female) were retro-orbitally injected with Evans blue dye (10 mg/ml in saline, 100 µl) containing either DMSO or DAPT (20 µM). Mice were anesthetized using an isoflurane nebulizer and immobilized on a microscope stage in an imaging chamber equilibrated to 37°C (schematic, Fig. s16). Vascular permeability images were acquired with a Leica HC FLUOTAR L 25x/0.95 W immersion objective on an upright Leica TCS SP8 multiphoton microscope equipped with a Spectra-Physics Insight DS+ laser tuned to 950 nm excitation and non-descanned emission detection at 680 nm. Vascular permeability was assessed beginning 20 minutes post injection and continued every five minutes up to one hour. The diffusive permeability coefficient was measured for 5 vessels per field of view as described above.

For bulk tissue vascular permeability measurements, inducible Notch1 endothelial cell knockout mice {CDH5-CreERT2(+):NOTCH1fl/fl} were used and their littermates {CDH5-CreERT2(-);NOTCH1fl/fl} as controls. At 4-weeks old, mice received tamoxifen (0.2 mg/day) intraperitoneally for 5 consecutive days. Two weeks after the start of Cre induction by tamoxifen, Evans blue dye (10 mg/ml in saline, 100 µl) was injected retro-orbitally. Thirty minutes post injection animals were euthanized by cervical dislocation under anesthesia and blood and tissue samples including the lung were harvested. Blood samples were clarified at 14,000 rpm for 5 min at 4°C; freeze-dried lung samples were weighed and incubated with 500 µl formamide at 56°C for 48 hours and clarified by centrifugation. Optical density readings at 620 nm (EB) and 740 nm (heme) were collected using a SpectraMax M5 spectrophotometer (Molecular Devices) and the concentrations of Evans blue were calculated based on the standard curve of Evans blue dye solution serial-diluted in formamide. Tissue Evans blue levels were normalized by tissue weight and blood Evans blue concentration and corrected for heme pigment contamination.

Policy information about studies involving human research participants

12. Description of human research participants

Describe the covariate-relevant population characteristics of the human research participants.

No human research conducted.